We are IntechOpen, the world's leading publisher of Open Access books Built by scientists, for scientists

6,900
Open access books available

185,000
International authors and editors

200M
Downloads

Our authors are among the

154
Countries delivered to

TOP 1%
most cited scientists

12.2%
Contributors from top 500 universities



WEB OF SCIENCE™

Selection of our books indexed in the Book Citation Index in Web of Science™ Core Collection (BKCI)

Interested in publishing with us?
Contact book.department@intechopen.com

Numbers displayed above are based on latest data collected.
For more information visit www.intechopen.com



Chapter 3

All Solid-State Passively Mode-Locked Ultrafast Lasers Based on Nd, Yb, and Cr Doped Media

Zhiyi Wei, Binbin Zhou, Yongdong Zhang, Yuwan Zou, Xin Zhong, Changwen Xu and Zhiguo Zhang

Additional information is available at the end of the chapter

http://dx.doi.org/10.5772/48775

1. Introduction

Mode-locking technique is a widely used method for generating ultrashort laser pulses. The mode-locked laser output is a sequence of equally spaced laser pulses. The pulse width is limited by the spectral range of the gain medium and inversely related to the bandwidth of the laser emission. Compared with the active mode-locking technique, passively mode-locked laser with saturable absorber is able to generate much shorter pulse with a simple configuration. In particularly, based on the passive mode-locking mechanism, the Kerr-lens mode locking (KLM) Ti:sapphire laser is recognized as the most important ultrafast laser source. Not only a series of commercial femtosecond lasers with Ti:sapphire crystal were released, but also lead to many innovations in science, such as frequency comb, laser wake field acceleration, attosecond science, laser micro-fabrication *etc*. However, the major drawback of Ti:sapphire laser is its green pump laser source. Currently available green lasers generated by frequency doubled Nd:YAG laser or by Argon laser are relatively bulky and expensive, which limits the practical application of ultrafast Ti:sapphire lasers.

With the remarkable progresses in the semiconductor saturable absorber mirror (SESAM) and laser diode technology, ultrafast laser sources with directly diode-pumped schemes and SESAM mode-locking have attracted more and more attentions because of the compactness and low cost compared to the well developed femtosecond Ti:sapphire laser. Nowadays, intra-cavity SESAM is widely used to start and maintain stable mode locking. Intense studies have been performed on this kind of lasers. Many efforts have been made to find new gain materials for ultrafast laser generations. Our research activity in this field is focused on the development of all solid-state passively mode-locked ultrashort lasers based on a variety of gain media with various wavelength ranges in the near-infrared. Several gain media doped with Nd, Cr or Yb, such as Nd:YVO_4, Nd:$GdVO_4$, Nd:$LuVO_4$, Nd:GSAG,

INTECH
open science | open minds

© 2012 Wei et al., licensee InTech. This is an open access chapter distributed under the terms of the Creative Commons Attribution License (http://creativecommons.org/licenses/by/3.0), which permits unrestricted use, distribution, and reproduction in any medium, provided the original work is properly cited.

Cr:forsterite, Cr:YAG, Yb:YAG, Yb:YGG, Yb:GYSO, Yb:LSO etc, have been tested. The results indicate a series of ultrafast laser sources with low cost, compact, simple and robust configuration in the picosecond and femtosecond regimes, which would find a wide range of practical applications.

2. Mode-locking mechanism passively mode-locked solid-state laser with a SESAM

By using an intra-cavity SESAM for passive mode locking, one has to choose the correct parameters of SESAM for a given laser system to get pure CW mode locking [2.1]:

$$\left|\frac{dR}{dI}\right| I < \frac{g_0}{l}\frac{T_R}{\tau_L}. \tag{1}$$

where R is the absorber reflectivity, I is the laser intensity, T_R is the cavity round trip time, g_0 is small signal gain of the laser, l is the total loss coefficient of the laser cavity, τ_L is the upper state lifetime of the laser. That is, the laser tends to operate in Q-switched mode-locking regime with a longer upper state lifetime, larger total loss, or shorter cavity length. In other words, the Q-switching can be suppressed for a large small-signal gain, or small loss, or large saturation intensity, or long cavity. For a fast saturable absorber, the condition is given by [2.1]:

$$\left|\frac{dR}{dE_p}\right| E_p < \frac{g_0}{l}\frac{T_R}{\tau_L}. \tag{2}$$

3. Overview for different solid-state laser materials

Solid-state mode-locked lasers are applied in various fields of physics, engineering, chemistry, biology and medicine *etc*, with application including ultrafast spectroscopy, metrology, superfine material processing and microscopy. To generate ultrafast laser pulses, the laser materials must meet a series of conditions. Firstly, a pump wavelength for which a good pump source is available. Secondly, small quantum defect and high gain of the materials can help get high laser efficiency. Furthermore, it is crucial for laser media to possess a board emission band, which is necessary to generate ultrafast pulses.

We divide materials for generation of ultrafast laser pulses into two types.

The first type is the ones that could only support picosecond laser pulses due to their limited gain bandwidth. Whereas, these laser materials commonly have excellent laser capabilities, such as good thermodynamic property and could be directly pumped by a diode laser with high power. The representative laser media are Nd^{3+} doped materials, which have been applied in diode-pumped energetic and efficient picosecond lasers and amplifiers. A SESAM mode-locked, Nd^{3+}:YAG laser with pulse width of 20 ps and output power of 27 W

has been reported [3.1]. Also, an Nd^{3+}:YVO_4 laser with 20 ps of pulse width and 20W of laser power was achieved [3.2]. Malcolm *et al* reported an additive pulse mode-locking (APM) Nd^{3+}:YLF laser, and 1.5 ps pulses were generated [3.3], which is the shortest pulse result by Nd^{3+} doped crystals.

Also, the Nd^{3+} laser on the $4F_{2/3}$– $4I_{9/2}$ transition with emission wavelengths of around 900–950 nm has attracted more and more interest because the quasi three-level pulsed laser could be used for lidar detection of water vapor in atmosphere [3.4]. Up to now, only few works have been reported on passively mode-locked laser on quasi three-level operating of Nd^{3+} doped materials. By Nd:$YAlO_3$ crystal, laser pulses centered at 930 nm with 1.9 ps pulse duration and 410 mW average power has been demonstrated with a Ti:sapphire pump laser[3.5]. With Nd:YVO_4 crystal, 8.8 ps pulses with 87 mW of power [3.6] and 3 ps pulses with 140 mW of power [3.7] centered at 914 nm were achieved, pumped by diode laser and Ti:sapphire laser, respectively.

Other than Nd^{3+} doped crystals, a commonly used host material doped with Nd^{3+} ions is Nd:glass. Different with crystals, glasses are significantly cheaper and have a smoother fluorescence spectrum, which support femtosecond laser pulses generation. As a well known example, laser pulses as short as 60 fs with the output power of 80 mW at the center wavelength of 1053 nm have been achieved with Nd: glass laser [3.8]

The other type of gain media have relatively broad emission spectra, but suffer from one or more unpopular physical properties (Ti:sapphire crystal is the outstanding exception). Yb-doped materials belong to this group. Compared with Nd-doped laser media, Yb-doped materials have attracted even more and increasing interest over the past few decades because of their small quantum defect (resulting a low thermal loading), simple electronic structure (avoiding such unwanted processes as excited-state absorption, up-conversion, and concentration quenching), long fluorescence lifetime (particularly advantageous for Q-switched lasers and high-power ultrashort pulse amplification) and broad absorption and emission bands (compared with Nd^{3+}). These media have been successfully applied in high-power diode-pumped all-solid-state ultrafast laser sources. Until now, extensive mode-locking researches have been reported with various Yb-doped crystals, such as garnet (Yb:YAG [3.9-10]), vanadate (Yb:$GdVO_4$ [3.11]), oxyorthosilicates (Yb:LSO [3.12-13], Yb:YSO [3.13]), tungstates (Yb:KGW [3.14], Yb:KYW [3.15], Yb:KLW [3.16], Yb:NYW [3.17]), borates (Yb:YAB, Yb:LSB, Yb:LYB, Yb:BOYS, Yb:GdCOB, Yb:YCOB)[3.18-23], fluorite (Yb:YLF) [3.24], sesquioxide (Yb:Sc_2O_3, Yb:Lu_2O_3, Yb:$LuScO_3$) [3.25-27], silicate(Yb:SYS) [3.28], niobate(Yb:CN) [3.29]. The short pulse duration of 47 fs has been reported with a Yb^{3+}: $CaGdAlO_4$ crystal [3.30] and the shortest pulse width of 35 fs has been obtained by a Yb:YCOB crystal [3.20].

Transparent ceramics fabricated by the vacuum sintering technique and nanocrystalline technology have the advantages of high doping concentration, easy fabrication of large size samples and high thermal conductivity. This kind of materials has been intensively investigated for the use in ultrashort pulse lasers [3.31-36]. The first reported mode-locked ceramic laser is a Yb:Y_2O_3 laser, which generated 210 mW laser pulses with 450 fs pulse

duration and a center wavelength of 1037 nm [3.32]. With the Yb:YAG ceramic, 286 fs pulses with 25 mW output power and 233 fs with 20 mW output power at center wavelength of 1030 nm and 1048.3 nm respectively were achieved [3.35],. Our recent work has boosted the output power from a femtosecond ceramic Yb:YAG laser to 1.9 W [5.19].

To further reduce the thermal effect, especially important for high power laser operation, the thin-disk gain media configuration has been developed. The geometry of the gain media is designed such that the thickness is considerably smaller than the laser beam diameter and the heat generated along with the lasing is extracted dramatically through the cooled end face [3.37-3.40]. Combined with the high absorption of the pump laser and long lifetime of the excited state of the Yb^{3+}-doped active materials, this thin disk laser operation has been a great success in a variety of Yb^{3+}-doped materials [3.41-3.47]. Thin-disk laser based on Yb-doped active materials is a good way to get efficient and high output power laser with excellent beam quality and will find wide applications.

Cr^{4+}:forsterite crystal is an important laser medium to generate ultrashort laser pulses around 1.3 μm. It could be pumped by Nd:YAG laser or Yb-doped fiber laser around 1064 nm. Cr^{4+}:forsterite crystal has wide luminescence spectrum from 1100 nm to 1500 nm [3.48]. Up to now, the shortest pulse duration with Cr^{4+}: forsterite laser is 14 fs [3.49]. Also, another Cr^{4+} doped material (Cr^{4+}:YAG) could be employed as the laser medium to obtain ultrafast laser pulses around 1.4 to 1.6 μm. The absorption spectrum of Cr^{4+}:YAG extends from 950 nm to 1100 nm, so it could share similar pump laser as the Cr^{4+}:forsterite laser. So far, the shortest pulse duration with Cr^{4+}:YAG laser is 20 fs and achieved by Kerr-lens mode locking technology [3.50].

4. Mode-locked Nd-doped lasers at quasi-three levels

4.1. Laser transition at quasi-three levels

Nd^{3+} ions was the first of the trivalent rare earth ions to be used in a laser, and Nd^{3+} doped materials have been remaining the most important laser medium until now. Laser operation has been obtained with this ion incorporated in at least 100 different host materials, and the commonly used host materials are YAG and glass. Take Nd: YAG for example, Figure 1 shows the energy level diagram of Nd^{3+} pumped by 808 nm. The ground state population was pumped to the energy level $^4F_{5/2}$, and then via radiationless transition transfers energy to $^4F_{3/2}$ level. The stimulated emission is commonly obtained at three different groups of transitions centered at 1.34, 1.06, and 0.946 μm, which result from $^4F_{3/2} \rightarrow {}^4I_{13/2}$, $^4F_{3/2} \rightarrow {}^4I_{11/2}$, and $^4F_{3/2} \rightarrow {}^4I_{9/2}$ transitions, respectively.

When radiation at $^4F_{3/2} \rightarrow {}^4I_{13/2}$ and $^4F_{3/2} \rightarrow {}^4I_{11/2}$ transitions, the upper and lower energy levels of pump and laser are separate, this is called four-level operation. Because the lower laser level is well above the ground state $^4I_{9/2}$ and can be quickly depopulated by multi-phonon transitions, there is no appreciable population density ideally in the lower laser level at room temperature. In that way, re-absorption of the laser radiation is effectively avoided and a lower threshold pump power can be achieved.

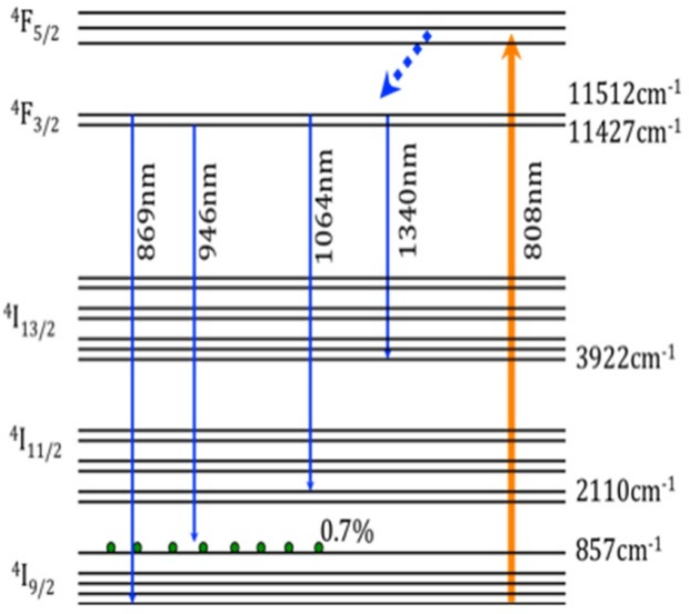


Figure 1. Energy level diagram of Nd:YAG

However, for $^4F_{3/2} \rightarrow {}^4I_{9/2}$ transition, the lower-laser level is the upper sub-level of the $^4I_{9/2}$ multiplet, so there is some population on the lower-laser level at room temperature. This is called quasi-three level operations. For example a thermal population of about 0.7 % in the lower laser level in Nd:YAG at room temperature. This sub-level is thermally coupled with the ground-state and should be efficiently populated with increasing temperature. This would induce a partial re-absorption loss of the laser radiation and cause an increase in the ground-state absorption loss, corresponding to an increasing in passive intra-cavity loss and laser threshold, result in the reducing of the laser output energy. In addition, the laser cross emission section of the quasi-three-level laser is dozens of times smaller than that of four-level system. Therefore, the laser operation with quasi-three levels is more difficult than that one with four levels.

As the typical Nd-doped laser medium, mode-locking researches on Nd:YAG laser for both quasi-three levels and four levels have been extensively reported, therefore, we only introduce our researches on mode-locking with some special Nd-doping media in this chapter.

4.2. Picosecond Nd:GSAG laser at 942nm for three levels operation

During the past few years, the Nd^{3+} laser on the $4F_{2/3}$– $4I_{9/2}$ transition has attracted wide interest because of emission wavelengths of around 900–950 nm. One important application for this quasi three-level pulsed laser is that it could be used for lidar detection of water vapor in atmosphere [3.4] because of characteristic absorption in the 935 nm, 942 nm, and 944 nm wavelength regions. Compared with optical parametric oscillators, generation of above wavelengths by Nd-doped crystal laser is much easier. Also, Frequency doubling of mode-locked quasi-three-level Nd^{3+} lasers generates picosecond blue pulses, which have potential application in many fields, such as life science, holography, and semiconductor inspection [4.1].

In the previous section, we have discussed the difficulty on quasi three-level operation compare with four-level operation. For Nd:GSAG here, a peak emission cross section of 2.7×10^{-20} cm^2 at 942.7 nm [4.2] and a peak emission cross section of 3.2×10^{-19} cm^2 around 1.06 μm [4.3] were determined by Kallmeyer *et al*. and Brandle *et al*., respectively. One can see the emission cross section at 942 nm is less than one-tenth the emission cross section at 1.06 μm. This leads to an increased threshold pump power and decreased optical conversion efficiency [4.3–5]. For the first time, we successfully a diode-pumped passively mode-locked Nd:GSAG laser with quasi-three-level operation at the central wavelength of 942.6nm [4.6]. The maximum output power is 510 mW at incident pump power of 16.7 W, and the pulses duration is short as 8.7 ps at a repetition rate of 95.6 MHz.

In the experiment, a standard z-fold resonator with end-pump configuration was employed as shown in Fig. 2. The pump source is a commercial fiber-coupled 808 nm LD with a core diameter of 200 μm, and an NA of 0.22. The crystal used in the experiment has dimensions of 4 mm×4 mm and Nd^{3+} concentration of 1 at. %. The both facets of the crystal have been antireflection (AR) coated at 942 nm, 808 nm and 1061 nm. The crystal was wrapped with indium foil and mounted on a water cooled copper heat sink and the water temperature was maintained at 10°C. Passive mode locking was started by using a SESAM (BATOP GmbH, Germany) with saturable absorptance of 4% at 940 nm, a saturation fluence of 70 μJ/cm^2, and relaxation time of less than 10 ps. The laser spot size on the SESAM is estimated to be 27 μm ×20 μm (tangential direction sagittal direction) using the ABCD matrix calculation. The dependence of the total output power on the incident pump power is shown in Fig. 3. Stable CW mode-locked laser can be obtained at the pump power above 11.5 W. When the incident pump power reached 16.7 W, the output power rose to 510 mW, corresponding to a optical efficiency of 3.1%, and the pulse energy inside the cavity and outside the cavity are about 88.3 nJ and 2.65 nJ, respectively. The high threshold pump power and the low efficiency are mainly due to the relatively high total transmission of 6% brought by the folded output coupler.

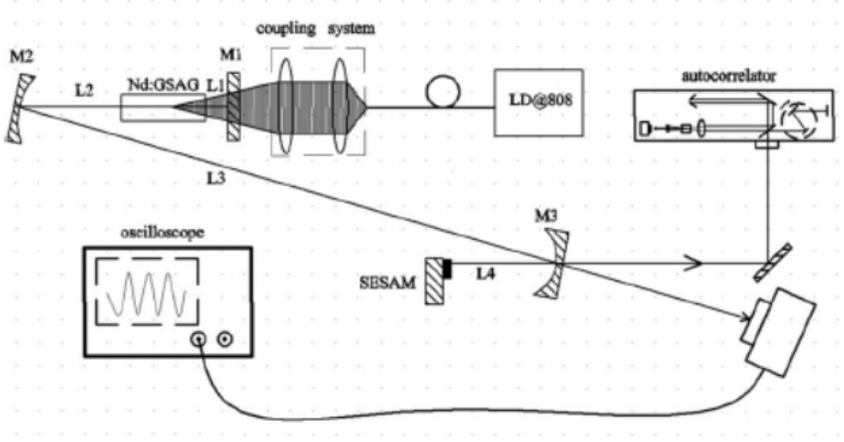


Figure 2. Schematic diagram of the experimental setup. Mirrors: M1: HT@808 nm and 1064 nm, HR@942 nm; M2: HR@942 nm, HT@1064 nm, radius of curvature (RoC)=500nm; M3: T=3%@942 nm, HT@1064 nm, RoC=100 nm.

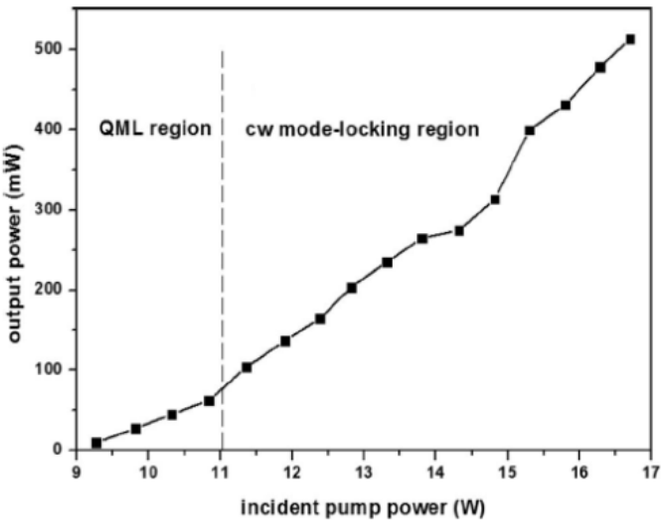
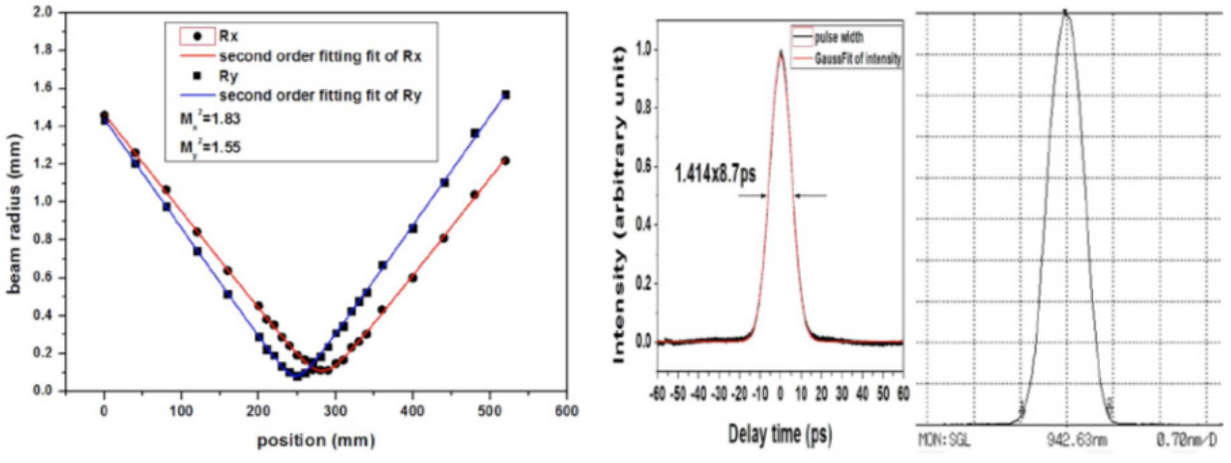


Figure 3. Dependence of the mode-locked laser output power on incident pump power.

The beam quality of the laser was measured with a CCD that could translate along a straight and slick track under incident pump power of 16.7 W. After fitting the measured data, as shown in Fig. 4 (a), we found that M^2 parameters were 1.83 and 1.55 for tangential direction and sagittal direction, respectively. The stable CW mode-locking regime held well for several hours and the repetition rate of the pulses was 95.6 MHz. The pulse duration was measured with an autocorrelator (FR-103MN, Femtochrome Research, Inc.) at the maximum output power, as shown in Fig. 4 (b). The pulse duration is about 8.7 ps assuming a Gaussian shape. Measured by an optical spectrum analyzer (AQ6315A, YOKOGAWA), the spectrum was centered at 942.6 nm which has an FWHM of about 0.65 nm, also shown in Fig. 4 (b). The time–bandwidth product of the pulses is 1.91, which is 4.3 times the transform limit for Gaussian pulses. The primary reason for this is that positive group-velocity dispersion introduced by crystal itself stretched the pulses.



(a) (b)

Figure 4. (a) Measured M^2 for tangential direction (Rx) and sagittal direction (Ry); (b) left: Intensity autocorrelation trace of the pulse; right: The laser spectrum of mode-locking operation.

4.3. Picosecond Nd:GGG lasers for both four levels and quasi-three levels

The Nd^{3+} doped gadolinium-gallium-garnet (GGG) crystal, a well known laser gain medium, was firstly reported in 1964 [4.7]. It has many desirable properties as a laser host material, such as excellent thermal conductivity, good mechanic properties, large thermal capacity, high doped concentration, and large size etc, as shown in Tab.1 [4.8-9]. With this laser medium, 30 kW average output power had been demonstrated from a solid-state heat capacity lasers (SSHCL) by Lawrence Livermore National Laboratory in 2004 [4.10]. Although Qin *et al* had obtained mode-locking operation at 1061 nm; the output power is only hundreds of milli-watt [4.11]. In this section, we described a diode pumped mode-locked Nd:GGG laser operation at both four levels and quasi-three levels transition. A laser pulse of 15 ps and 24 ps were generated with an average power of 3.2 W and 320 mW at 1062 nm and 937.5 nm, respectively [4.12-13].

Chemical formula	$Nd:Gd_3Ga_5O_{12}$
Crystal Structure	Cubic
Lattice Constant	a=1.2376 nm
Melting point	1725 °C
Density	7.1 g/cm^3
dn/dT ($\times 10^{-6}$/K)	17
Thermal conductivity	7 W/mK
Heat capacity	0.38×10^3 Ws/(Kg•K)
Thermal expansion coefficient	8×10^{-6}/ °C
Laser Transition	$^4F_{3/2} \rightarrow {}^4I_{11/2}$ 1062 nm $^4F_{3/2} \rightarrow {}^4I_{13/2}$ 1331 nm $^4F_{3/2} \rightarrow {}^4I_{9/2}$ 937.5 nm
Emission cross section at 1061 nm	$2.7\text{-}8.8\times10^{-19}$cm^{-2}
Fluorescence lifetime	240 μs
Absorption band	808 nm
Photon energy at 1.06 μm	$h\nu = 1.86 \times 10^{-19}$ J
Index of refraction	1.94

Table 1. Properties of Nd:GGG crystal

Laser operation was performed by using a 5-mm-long, antireflection-coated, 0.5 at. % doped Nd:GGG crystal. A high brightness fiber-coupled diode laser, with a core diameter of 200 μm and a numerical aperture of 0.22, was used as pump source. For ease of use, we designed a typical resonator as shown in Fig. 5 for four level running. Passive mode locking was started by a SESAM, which has a saturable absorption of 4% at 1060 nm and a saturation fluence of 70 μJ/cm^2. A plane-wedged mirror with transmission rate of 10 % was used as the output coupler (OC). With this configuration, the laser mode radii in the crystal and on the SESAM were calculated to be 98μm and 105 μm, respectively.

After the optimized alignment, stable mode-locking operation with single mode output was obtained when the incident pump power exceeded 15 W. We measured the intensity

autocorrelation trace by using a commercial noncollinear autocorrelator (FR-103MN, Femtochrome Research, Inc.). As shown in Fig. 6 (a), the FWHM width of the autocorrelation trace is about 23 ps. If a sech^2-pulse shape is assumed, the mode-locked pulse duration is 15 ps. The central wavelength locates at 1062.5 nm with spectrum bandwidths of 0.25 nm. The time-bandwidth product was calculated to be 0.997, which was about 3 times the transform limit for Gaussian pulses.

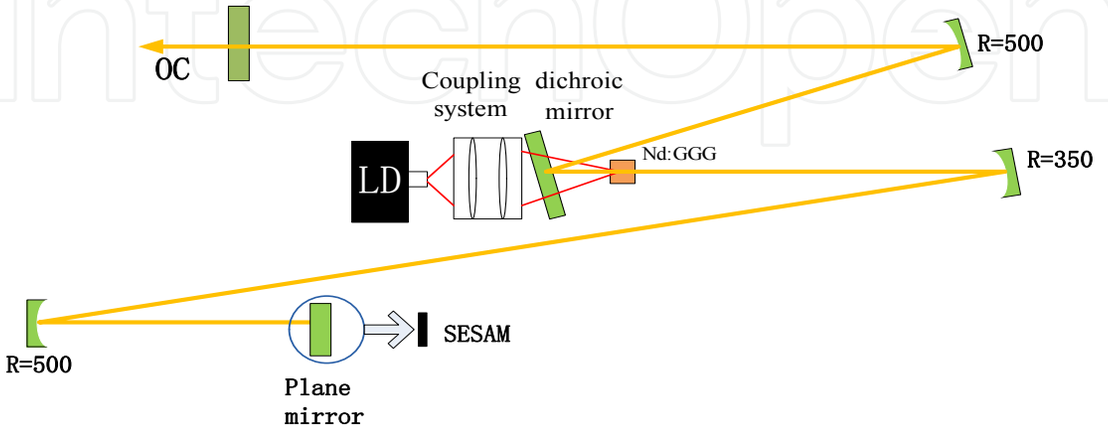


Figure 5. The Experimental layout of passively mode-locked for Nd:GGG laser operating at four level transition.

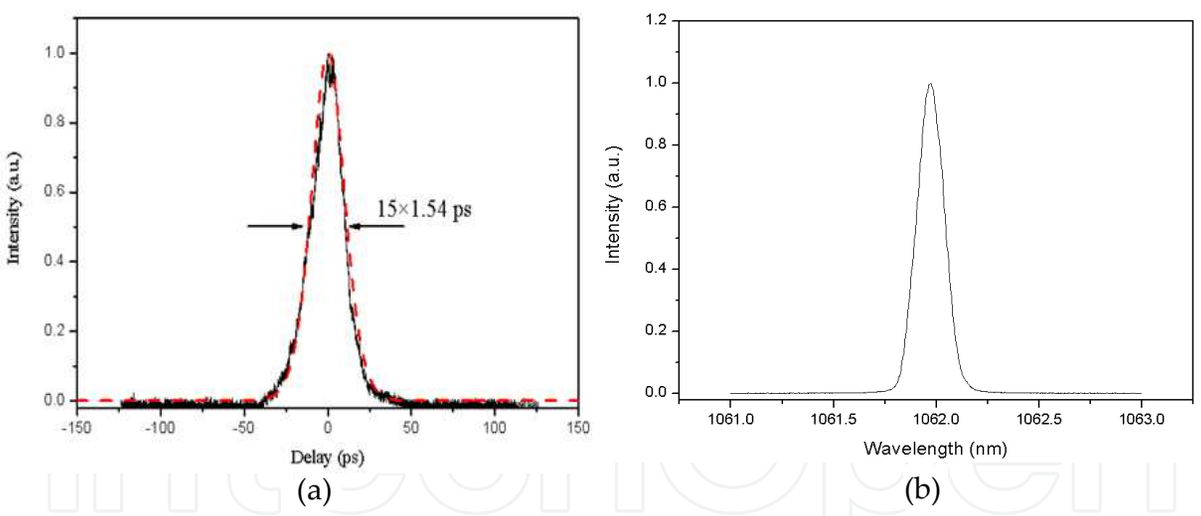


Figure 6. (a) Intensity autocorrelation trace of the pulse; (b) the laser spectrum of mode-locking operation

Mode-locking Nd:GGG laser at quasi-three level transition was realized with the same pumping source and the laser crystal. In order to reduce loss, a simple Z-folded cavity consisted of four mirrors was employed, as shown in Fig.7, the total cavity length was approximately 1.82 m corresponding to a repetition rate of about 82 MHz. To suppress parasitic oscillation at 1.06 μm, most of the cavity mirrors were antireflection coated at this wavelength. A similar SESAM from same company was used to start the mode-locking. For optimization of the cavity alignment, a plane mirror coated for high reflection at 940 nm was

used as an end mirror. The waist radii of the laser mode in the crystal and on the SESAM were design to be 80 μm and 20 μm for mode match, respectively. The stable pulses train with the maximum output power of 320 mW has been obtained under the incident pump of 20 W.

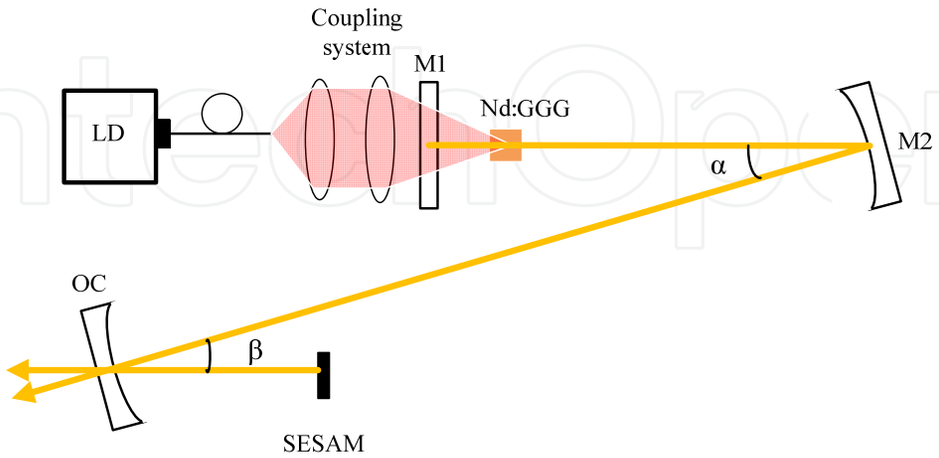


Figure 7. Scheme of Nd:GGG laser mode-locked at quasi-three-level transition.

Intensity autocorrelation trace shown that the FWHM width of the autocorrelation trace is about 39.3 ps (Fig. 8 (a)). If a Gaussian-pulse shape is assumed, the mode-locked pulse duration is 27.8 ps. Fig. 8 (b) depicts the output spectrum at the stable mode locking which was centered at 937.5 nm and had a bandwidth of 0.14 nm. This resulted in a time–bandwidth product of 1.33 which was 3 times the transform limit for Gaussian pulses. The high time-bandwidth product may be resulted from the high group delay dispersion of the laser crystal [4.14].

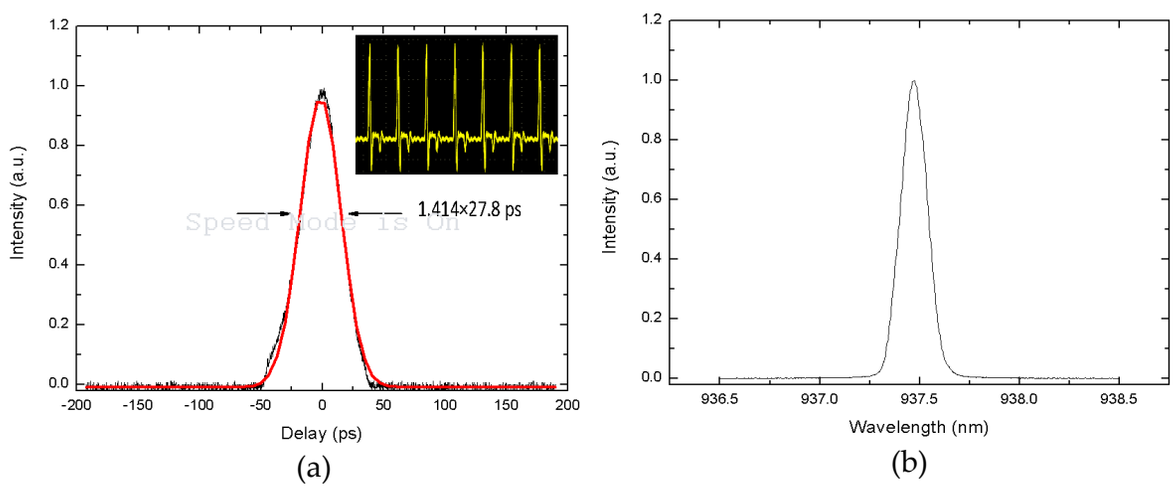


Figure 8. (a) Intensity autocorrelation together with Gaussian fit curve shows the pulse width of 24.7 ps. The inset is oscilloscope traces of the CW mode-locked pulse train. The laser spectrum of mode-locking operation.

4.4. Picosecond Nd:$GdVO_4$ at 912nm for three levels operation

As the most efficient laser host medium, the Nd:YVO_4 crystal has been widely used for diode-pumped mode-locking laser research [4.15-20]. Compare to Nd:YVO_4 crystal, Nd:$GdVO_4$ possesses many significant advantages such as higher thermal conductivity, larger absorption cross-section and larger stimulated emission cross-section [4.21]. In addition, Nd:$GdVO_4$ emits the shortest wavelength radiation on the $^4F_{3/2} - {}^4I_{9/2}$ transition for its smallest splitting (409 cm^{-1}) of the lower laser level. However, the quasi-three levels laser is more difficult to operate than the four level laser and would cause the increase in ground-state absorption loss and laser threshold, and then reducing the output energy of the laser.

In the past, much more attention had been paid on passively Q-switched and mode-locked lasers with Nd:$GdVO_4$ crystal operating at 1064 nm and 1342 nm [4.22-26]. However, passively mode-locked Nd:$GdVO_4$ laser at quasi-three-level were less reported. H. W. Yang et al have reported a passively Q-switched Nd:$GdVO_4$ laser at 912 nm with V^{3+}:YAG as the saturable absorber [4.27]. Fei Chen *et al* have obtained passively Q-switched mode-locked Nd:$GdVO_4$ laser at 912 nm [4.28]. In 2006, our group successfully demonstrated the CW passively mode-locked Nd:$GdVO_4$ laser for three level laser operation [4.29]. In this section, we present a stable CW mode-locked Nd:$GdVO_4$ laser at 912 nm with the total output of 128 mw and the pulse width of 6.5 ps [4.30].

We employed a four-mirror folded cavity, shown in Fig. 9. The pump source is a commercially available fiber-coupled diode-laser which could emit a rated maximum power of 30W at 808 nm, with a core diameter of 200 μm and a N.A. of 0.22. The dimensions of the crystal are 3×3×4 mm^3 with a concentration of 0.2 at%. The crystal was coated and wrapped with indium foil and then mounted in a water-cooled copper block. The water temperature was maintained at 10 ℃. The SESAM (Batop GmbH, Germany) used for mode-locking is with a modulation depth of 2% at 912 nm and a saturation fluence of 70 μJ/cm^2. A plane mirror coated HR at 912 nm replaced the SESAM, and then the laser was operating at 912 nm. The maximum output power of 1.45 W was obtained with an incident pump power of 20.3 W. Then we put the SESAM instead of the plane mirror in the cavity. At pump power above 13.4 W, a stable CW mode-locking state was observed. The repetition rate was 178 MHz and the maximum output power was 128 mw at a pump power of 19.7 W, as shown in Fig.10.

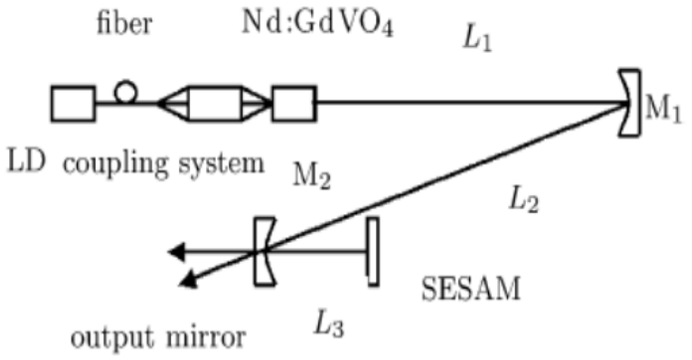


Figure 9. Schematic diagram of the passively mode-locked 912 nm Nd:$GdVO_4$ laser.

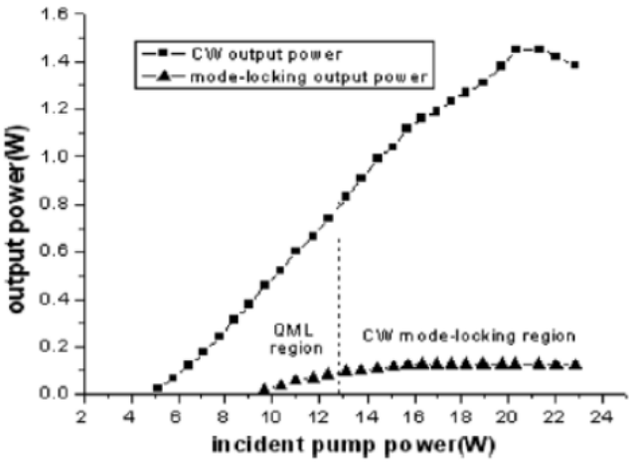


Figure 10. Dependence of the laser CW output and mode-locking output on the incident pump power. QML: Q-switched mode-locking.

The pulse width was measured with a homemade non-collinear second-harmonic-generation autocorrelator. The trace of the SHG autocorrelation is shown in Fig. 11. Assuming a Gaussian pulse profile, we estimated the pulse duration to be approximately 6.5 ps. The corresponding spectrum was measured, it has two peaks at the central wavelengths of 912.3 nm and 912.7 nm, respectively, and the both corresponding bandwidths were 0.25 nm (FWHM).

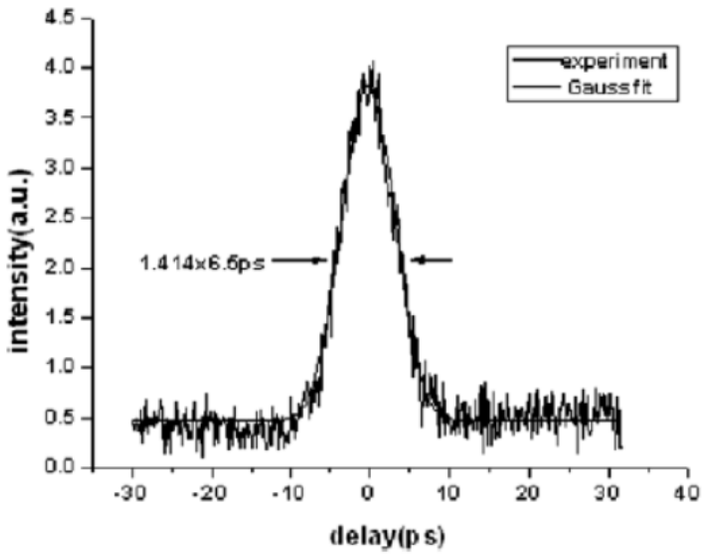


Figure 11. The measured autocorrelation trace of the pulses of the passively mode-locked 912 nm Nd:$GdVO_4$ laser.

4.5. Nd:$LuVO_4$ laser at 916 nm for three levels operation

As in vanadate family, Nd:$LuVO_4$ has larger absorption and emission cross sections than those of Nd:YVO_4 and Nd:$GdVO_4$, and thus has attracted much attentions. By employing the Nd:$LuVO_4$ crystal (length of 5.5 mm and doping with 0.1 at.% Nd^{3+} concentration) and

using the similar Z-folded cavity design as in passively mode-locked Nd:$GdVO_4$ laser, we obtained a stable passively cw mode-locked Nd:$LuVO_4$ laser at 916nm [4.31]. The pulses train has 6.7 ps of pulse duration (shown in Fig. 12) at repetition rate of 133 MHz. The average output power was 88mW under the pump power of 17.1 W.

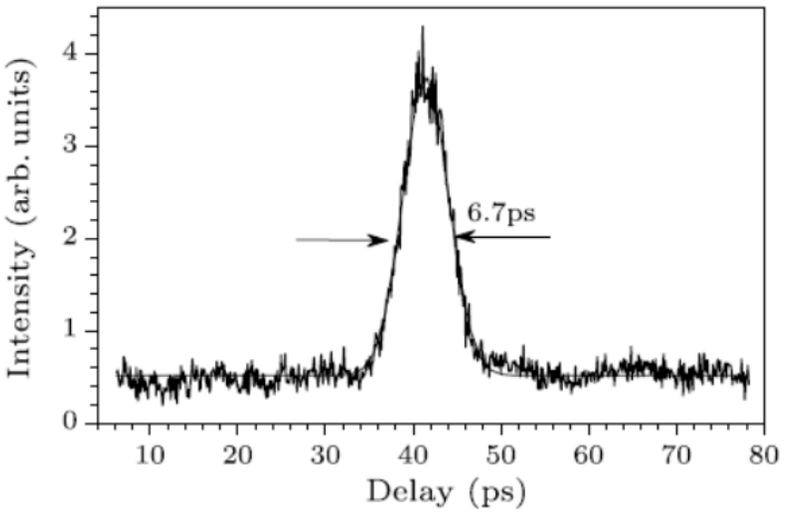


Figure 12. Autocorrelation trace of the mode-locked Nd:$LuVO_4$ laser.

5. Mode-locked femtosecond and picosecond Yb-doped laser

The Yb^{3+}-doped materials have excellent advantages among the available laser hosts, such as high quantum efficiency, absence of excited-state absorption, direct diode laser pumping, as well as large emission bandwidth which can support femtosecond pulses generation, and so on. Up to now, extensive mode-locking research has been reported with various Yb-doped materials. In the following section, we will present some numerical and experimental studies on several passively mode-locked Yb-doped lasers.

5.1. Numerical and experimental investigation of the Yb:YAG laser at a wavelength of 1.05 μm

Among a variety of Yb-doped crystals, the Yb:YAG crystal is one of the most important laser media for several important advantages: excellent thermal-mechanical properties, ease of growth in high-quality crystal, and a high doping concentration without quenching, etc. Remarkable progress has been achieved with ultrashort Yb:YAG lasers because of these favorable properties [5.5, 5.6]. Typically, the Yb:YAG crystal has two main emission wavelengths, 1.03 and 1.05 μm respectively. Ultrafast Yb:YAG laser operating at 1.05 μm has special advantages compared with the one at 1.03 μm. First, the gain around 1.05 μm is flatter and can support femtosecond pulses with broader spectrum and shorter pulse width. Yb:YAG laser pulses as short as 100 fs have been demonstrated at this wavelength. In contrast, limited by the width of the narrow gain peak at 1030 nm, the shortest pulse achieved at this wavelength has the width of 340 fs [5.7], and most femtosecond pulses are

longer than 500 fs [5.5, 5.6]. Second, ultrashort pulses at 1.05 μm can be useful in high energy glass laser facilities as the seeding source.

To obtain oscillation at 1.05 μm by the Yb:YAG laser, one must suppress the oscillation at 1030 nm. Some researchers use specially coated mirrors to distinguish these two neighboring wavelengths [5.7,5.8], which, however, inevitably brings additional cavity losses and leads to low laser efficiency. Investigations on the preferred emission wavelength versus the length and the ion concentration of the Yb:YAG crystal will be discussed below, we also described a novel method to obtain efficient 1.05 μm operation based on the Yb:YAG laser[5.9,5.10].

5.1.1. Theoretical investigation

The electronic diagram of the ytterbium ion is shown in Figure 13. It's a typical quasi-three-level system. As the zero phonon line is very narrow and the corresponding absorption cross section is lower, the most efficient pump transition for Yb:YAG is l_1 to u_2 at 940 nm. Emission transitions are from u_1 to l_2 (1024 nm), to l_3 (1030 nm) and to l_4 (1050 nm). For quasi-three-level longitudinally pumped laser system, the thickness of the gain medium is more crucial for the laser oscillation than in a four-level system. In a quasi-three-level system, the terminal level of the laser transition is thermally populated. Thus minimum pump intensity is required for reaching population inversion. As the pump is absorbed when traveling in the gain medium, this minimum intensity is reached after a crystal length which is the so-called optimum length. In the following, the different optimum length at different oscillation wavelength in the Yb:YAG laser will be investigated by the model developed in [5.11] and [5.12].

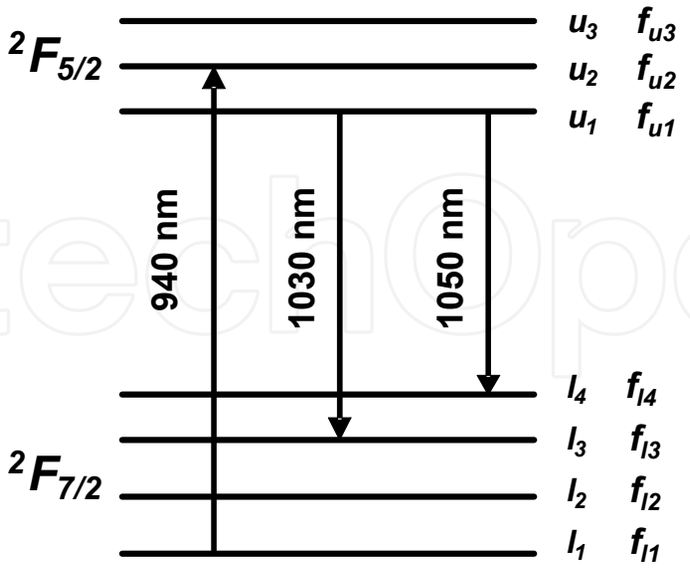


Figure 13. Energy level diagram of Yb^{3+} ion in the Yb:YAG crystal.

The amplification of the laser wave and the absorption of the pump wave are described by equations (5.1a) and (5.1b):

$$\frac{dI_l^{\varepsilon}}{I_l^{\varepsilon}} = \varepsilon g_0 \{X_u - f_l\} dz \tag{3a}$$

$$\frac{dI_p^{\varepsilon'}}{I_p^{\varepsilon'}} = -\varepsilon' \alpha_0 \{f_p - X_u\} dz \tag{3b}$$

where X_u is the population density of the excited state. $X_u = N_u/N_{Yb}$. N_u is the population of the excited state and N_{Yb} is the Yb^{3+} ions concentration. The linear coefficients of gain g_0 and absorption α_0 are given by equations (4):

$$g_0 = \sigma_l N_{Yb}(f_{lk} + f_{u1}) \qquad \alpha_0 = \sigma_p N_{Yb}(f_{l1} + f_{uj}) \tag{4}$$

with $f_l = \frac{f_{lk}}{f_{lk} + f_{u1}} \qquad f_p = \frac{f_{l1}}{f_{l1} + f_{uj}}$,

where σ_P and σ_l are the absorption and emission cross sections, and f_{jk} are the Boltzmann partition factors of the sublevel k of the manifold j, ε and ε' are ±1 relative to the direction of propagation of the laser and the pump beams respectively. The dynamic equation for the population reads:

$$\tau_u \frac{dX_u}{dt} = I_p(f_p - X_u) - X_u - I_l(X_u - f_l) \tag{5}$$

where τ_u is the excited state life time and I_p and I_l are the pump and laser intensity travelling in both directions normalized to the saturation intensity given by (6):

$$I_{sat}^{l} = \frac{h\nu_l}{(f_{lk} + f_{u1})\tau_u \sigma_l} \qquad I_{sat}^{p} = \frac{h\nu_p}{(f_{l1} + f_{uj})\tau_u \sigma_p} \tag{6}$$

In CW regime, equation (5) reads: $I_p(f_p - X_u) - X_u - I_l(X_u - f_l) = 0$. Then:

$$X_u = \frac{f_p I_p + f_l I_l}{1 + I_p + I_l} \qquad I_i = I_i^+ + I_i^- \tag{7}$$

With regard to equation (3a), the laser beam is reabsorbed when $X_u < f_l$. Then minimum pump intensity required for bleaching the amplifier medium is given by:

$$X_u = f_l \qquad I_p^{\min} = \frac{f_l}{f_p - f_l} \tag{8}$$

For single pass pumping where the pump is travelling following one direction, the pump transmission required for inverting the amplifier medium is given by:

$$I_p(0)\Gamma = I_p^{\min} \qquad \Gamma = \beta = \frac{I_p^{\min}}{I_p(0)} \tag{9}$$

As the pump is absorbed when traveling in the amplifier, this minimum intensity required for bleaching the amplifier medium at the laser wavelength is reached after an amplifier length we call optimum length.

For single pass pumping and CW laser, the output intensity has been derived in [5.12]:

$$I_{out}(L) = (1-R_s)\sqrt{R_m}\,\frac{g_0\left(\dfrac{I_p(0)(1-\Gamma)}{\alpha_0} - f_l L\right) + \ell n\sqrt{R_m R_s}}{\left(1-\sqrt{R_m R_s}\right)\left(\sqrt{R_m}+\sqrt{R_s}\right)} \tag{10}$$

Where R_s and R_m are the reflectivity of the output and rear mirror respectively (assuming all the losses of the cavity are taken into account in the loss of the rear mirror). By (3a) and (3b), it is possible to find a relation connecting the pump and the laser intensities. Then, Γ reads:

$$\Gamma = \sqrt{R_m R_s}^{-\frac{\alpha_0}{g_0}} \exp\left\{-\alpha_0\left(f_p - f_l\right)L\right\} \tag{11}$$

The optimum length for which the laser wave is not reabsorbed leads to maximum output power. Then, the pump transmission must be equal to β leading to:

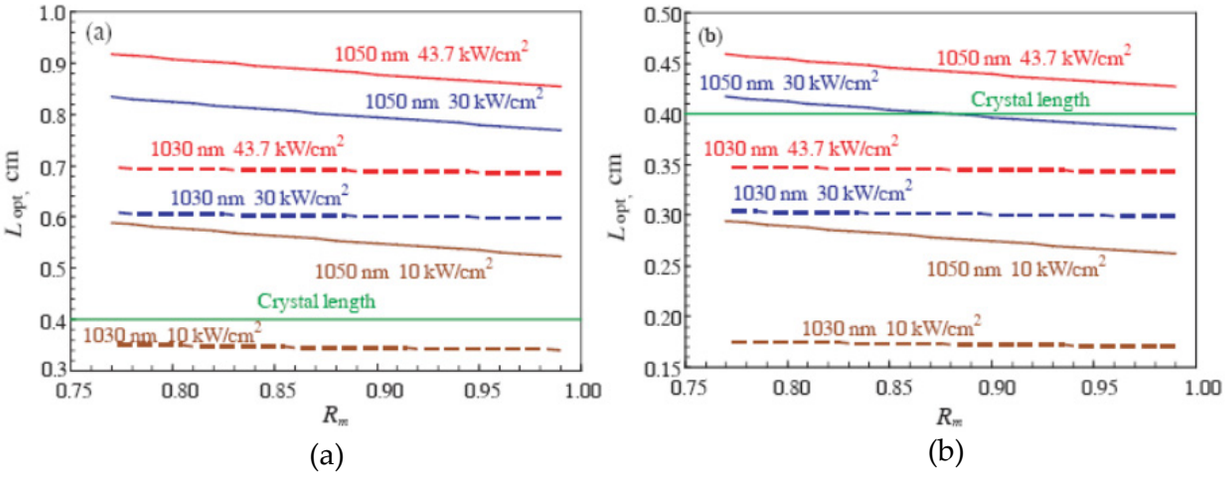
$$L_{opt} = \frac{-1}{f_p - f_l}\,\ell n\left\{\sqrt{R_m R_s}^{\frac{1}{g_0}}\,\beta^{\frac{1}{\alpha_0}}\right\} \tag{12}$$

This result can also be obtained by computing the length for which $I_{out}(L)$ is maximum using formula (10). In CW laser operation of a three-level system, inversion density of gain media remains constant above laser threshold. Then, for a given laser medium, pump transmission is fixed and determined by cavity loss level and spectroscopic parameters of gain media. It is worth to mention that L_{opt} as well as β depends on the pump intensity.

	Absorption	Emission	
λ (nm)	940	1030	1050
f_u+f_l	1.04E+00	0.75	7.00E-01
σ (cm^2)	7.60E-21	3.30E-20	4.80E-21
τ_u (ms)	0.95	0.95	0.95
f_i	0.838	0.0626	0.0205

Table 2. Values of the crystal parameters

Now the length and the ion concentration of the crystal can be investigated to find out that under what kind of condition the laser oscillation at 1050 nm can be preferred. The emission transitions of Yb: YAG are from upper level u_1 to lower level l_3 (1030 nm) and l_4 (1050 nm). First, as the l_4 energy level is higher than the l_3 one, its thermal population is lower and the f_l parameter at room temperature is 0.0284 against 0.0646. Then, the corresponding optimum crystal length is larger and more pump energy is absorbed. Using (10), the optimum crystal length versus the rear mirror reflectivity for various pump intensities can be calculated. The values of the crystal parameters used for the computation are reported on Table 2. The cross sections are spectroscopic cross sections [5.13].



(a) (b)

Figure 14. Optimum length versus reflectivity of the rear mirror for various pump intensities with (a) 5% and (b) 10% doping.

Figure 14 shows the calculated optimum lengths for the two wavelengths of 1030 and 1050 nm and for 5 at. % (a) and 10 at. % (b) doping concentration. It can be noticed that, for a crystal length of 4 mm with 5 at. % doping, the crystal length is much lower than the optimum lengths for 1050 nm oscillation at different pump intensities, but close to the 1030 nm optimum length. As a result, oscillation at 1030 nm is favored. It shows good agreement with the results reported in [5.7]. In that paper, a 5%-doped, 3.5-mm-long Yb:YAG crystal was used, and under the pump intensity of about 36 kW/cm², laser oscillation was achieved at the wavelength of 1030 nm. But for the 10 at. % doped crystal, one can notice that the situation is different. The preferred crystal length is much shorter than that of 5 at. % doping crystal. Only when the crystal is very short, oscillation at 1030 nm will be preferred. If the crystal length reaches a proper value, such as 4 mm, the 1030 nm laser is more likely to be re-absorbed and suppressed. This indicates a new way to suppress 1030 nm and get the oscillation at 1050 nm only by choosing the Yb:YAG crystal with proper ion concentration and optimized length.

5.1.2. Mode-locked Yb:YAG laser at the wavelength of 1.05 μm

The experiment is performed with a 10 at. % doped Yb:YAG crystal with the length of 4 mm. A typical Z-shape cavity was used (Figure 15(a)). All the coatings of the intra-cavity mirrors

are identical for 1030 and 1050 nm. A CW Ti:sapphire laser at 940 nm with 2 W power was used as the pump. The pump intensity at the front face of the crystal is calculated to be about 43.7 kW/cm^2 at 2 W pump power. The measured absorption of the crystal to the pump light is 91 %, which is in good agreement with the theoretically calculated value of 92.6% from equation (9) by the model.

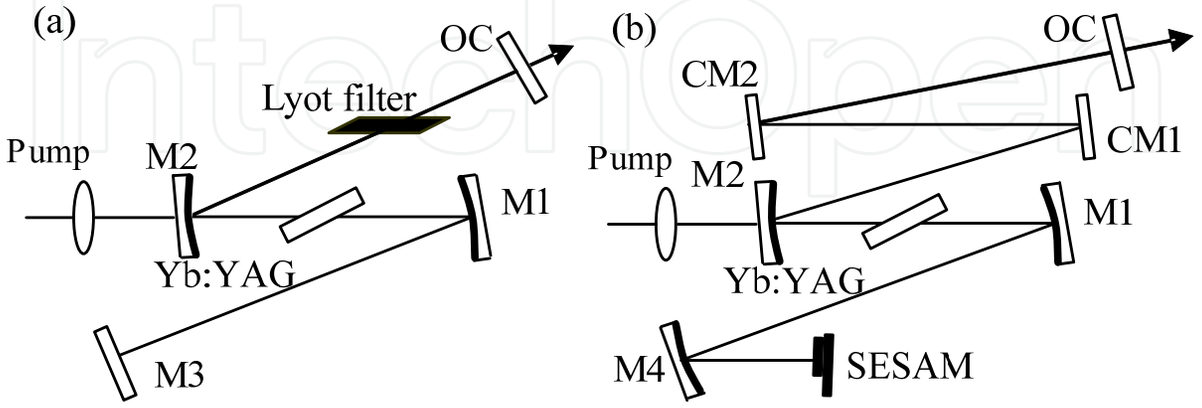


Figure 15. Cavities used to study the (a) CW and (b) mode-locked laser performance of a Yb:YAG laser.

For CW operation, two kinds of output couplers were used, with the transmittivity of 1% and 2.5% respectively. The wavelength of the free-running laser was measured with a scanning spectrometer. When the pump power was increased from the threshold power to 2 W, the emitting wavelength was keeping at 1050 nm. This can be well explained by Figure 14(b). When the pump intensity was increased from zero to 43.7 kW/cm^2, the length of the crystal is near the optimum length of 1050 nm oscillation and much longer than that of 1030 nm oscillation. 1030 nm lasing is more likely to be reabsorbed and oscillation at the wavelength of 1050 nm can be preferred. Under the pump power of 2 W, the maximum output power was as high as 650 mW, leading to a slope efficiency as high as 45.8%.

Based on the CW 1050 nm operation, the passively mode-locking operation of this laser was also investigated. The cavity layout is shown in Figure 15(b). An output coupler with 0.5% transmittivity was used in this setup. Without intracavity dispersion compensation, stable mode-locked pulses in picosecond regime were obtained. A typical intensity autocorrelation trace (obtained by an FR-103MN autocorrelator, Femtochrome Research, Inc.) of the output pulses is shown in Figure 16(a). Assuming a sech^2 pulse shape, one can obtain the FWHM pulse duration of 1.8 ps. A simultaneous measurement of the pulse spectrum is illustrated by the insertion.

A pair of Gires-Tournois interferometer (GTI) mirrors, which introduce group delay dispersion (GDD) of -1200 fs^2 from 1020 to 1080 nm by single pass, were used to obtain femtosecond laser operation. It's enough to compensate the positive GDD caused by the Yb:YAG crystal and the net intracavity GDD remain at a minus value. With this alignment, stable self-starting soliton-like pulses were obtained. Figure 16(b) shows the measured autocorrelation trace and the spectrum of the pulses. The pulse width is 170 fs assuming a sech^2-shape pulse and the FWHM spectral bandwidth reaches 7 nm. The central wavelength

redshifted from 1050 to 1053 nm. It's worth to mention that the central wavelength of this femtosecond Yb:YAG laser is exactly the working wavelength of high energy Nd:glass based ultrafast amplifier system. It indicates that the femtosecond Yb:YAG laser has the potential to be an excellent seed source for the above system. Under the full pump power of 2 W, the average power of the femtosecond pulses is 180 mW at a repetition rate of 80 MHz, corresponding to the peak power of 13.3 kW.

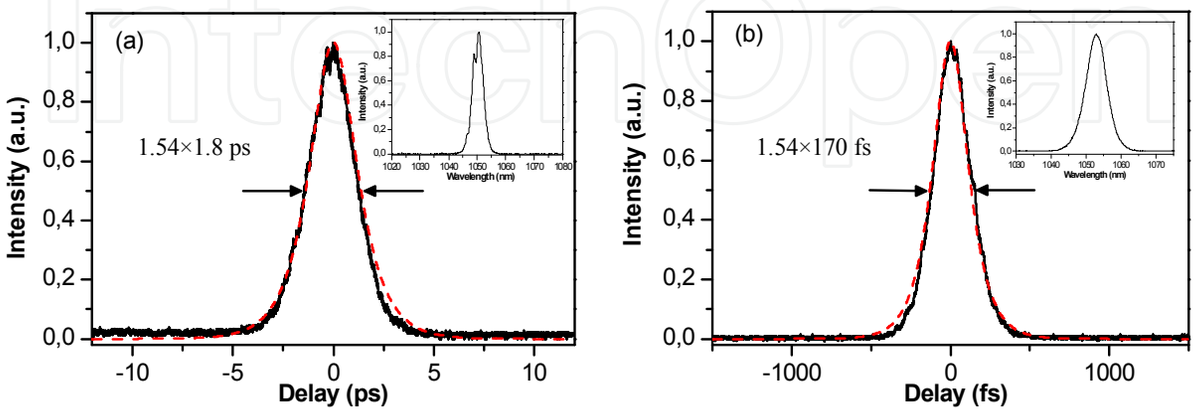


Figure 16. (a) Intensity autocorrelation trace of the picosecond pulses; inset, the corresponding laser spectrum. (b) Intensity autocorrelation trace of the femtosecond pulses; inset, the corresponding laser spectrum.

5.2. Diode-pumped efficient femtosecond ceramic Yb:YAG laser and picosecond Yb:LSO laser

Highly transparent Yb:YAG ceramics for solid-state laser gain medium have been developed in recent years, by the vacuum sintering technique and nanocrystalline technology [5.14]. This Yb:YAG ceramics have such advantages as favorable mechanical properties [5.15], high doping concentration, low cost, and easy fabrication of large-size samples. All of these advantages promise Yb:YAG ceramic extensive potential for the development of high-efficiency and high-power ultrafast laser.

In the first Yb:YAG ceramic laser experiment [5.14], the cw output power was 345 mW with a slope efficiency of 26%. With the improvement on the Yb^{3+} doping concentration, excellent cw laser performances by Yb:YAG ceramics have been demonstrated. Dong et al. realized a 1.73 W cw output power with the absorbed pump power of 2.87 W, corresponding to a slope efficiency as high as 79% [5.16]. A cw output power as high as 6.8 W with the slope efficiency of 72% was further demonstrated by Nakamura et al [5.17]. In the pulsed operation, Yoshioka et al. demonstrated the first mode-locked operation of a Yb:YAG ceramic laser [5.18]. The reported efficiency for the femtosecond operation was, however, relatively low; the output power was 250 mW at the pump power of more than 26 W.

In this section, a high-power and high-efficiency operation of a diode-end-pumped femtosecond Yb:YAG ceramic laser will be described [5.19]. For self-starting femtosecond laser operation, more complicated cavity configuration is needed than for CW laser

operation. Lots of additional cavity losses are thereby introduced, such as the insertion losses by the prisms, the non-saturable loss by the SESAM, and the broadband reflection losses by intra-cavity reflectors, etc. To obtain efficient mode-locking operation, several major improvements were made compared with Ref. 5.17. First, other than prisms, highly reflective negative-dispersion mirrors were adopted for dispersion compensation. This avoided the insertion losses by the prisms, which usually caused low efficiency in mode-locked Yb-doped solid-state lasers. Experimental results on this kind of lasers have shown the significant efficiency increase by negative-dispersion mirrors replacing prisms [5.20, 5.21]. Second, a piece of SESAM with the non-saturable loss parameter as low as 0.3% was used to further minimize the intra-cavity losses. Third, the transmission of the output coupler mirror was also optimized for femtosecond operation. Finally, high pumping intensity is much helpful to obtain efficient laser operation. For this purpose, a 7-W high brightness fiber coupled diode laser (Jenoptik laserdiode GmbH) at 968 nm was adopted as the pump. The fiber core diameter is 50 μm, with a numerical aperture of 0.22.

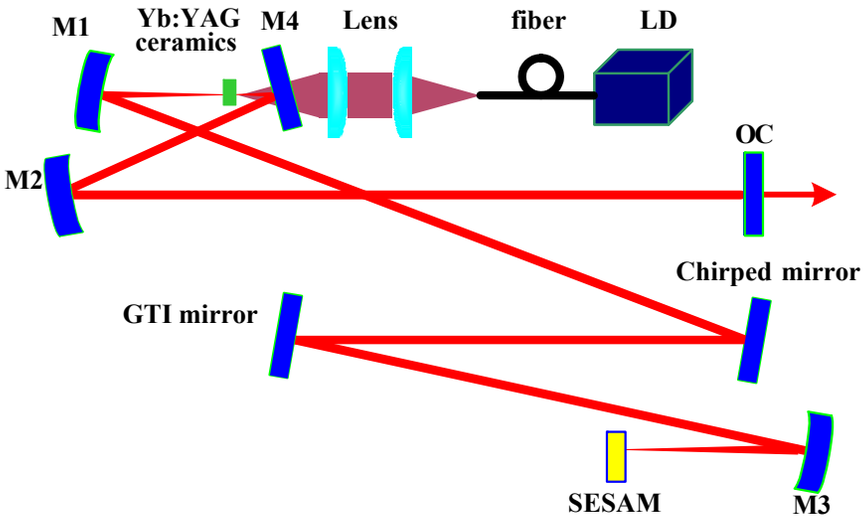


Figure 17. Schematic of the mode-locked Yb:YAG ceramic laser.

A schematic of the laser cavity and pump geometry is shown in Figure 17. The pump laser was reimaged into the Yb:YAG ceramic through a coupling system. The cavity was a standard Z-shape structure, with a piece of high reflective plane mirror folding one arm of the cavity to fit the short focusing length of the pump light. M1 and M3 were curved folding mirrors with ROC of 200 mm, and M2 with ROC of 300 mm. A 2-mm-long 10 at. % doped Yb:YAG ceramic was used for the gain medium. The absorption of the ceramic to the pump laser was around 50% in the experiment due to the lower and narrower absorption peak at 968 nm than at 940 nm. Negative dispersion was introduced by a Gires-Tournois interferometer (G-TI) mirror and a chirped mirror. The G-TI mirror provides second-order dispersion compensation of about -1000 ± 300 fs^2 per rebound in the spectral range from 1030 to 1050 nm and the chirped mirror provides -120 ± 20 fs^2 from 1000 to 1100 nm. The cavity was designed to sustain a fundamental mode with a beam waist of 65 μm × 67 μm in the crystal, and a waist of 58 μm × 65 μm on the SESAM. The total cavity length corresponds to a repetition rate of 64.27 MHz.

Different mirrors were used as output couplers with transmissions of 1%, 2.5%, and 4% from 1020 to 1080nm. Stable soliton mode-locking regime was observed with 1% and 2.5% output couplings. With 4% coupling, the output power under the maximum pump was slightly higher than the output power by the 2.5% coupler, however, cw mode-locking couldn't be realized at this coupling condition. Figure 18 shows the output power as a function of the absorbed pump power for these two output couplers. With the decreasing of mirror reflectivity from 99% to 97.5%, the threshold incident pump power for cw mode-locking operation increased from 1.9 to 2.5 W. The maximum CW mode-locked output power was achieved with the 97.5% reflectivity output coupler. Under the incident pump power of 7 W (the measured absorbed pump power was 3.5 W), stable mode-locked output power of 1.9 W was obtained, corresponding to a slope efficiency of 76% with respect to the absorbed pump power. With the 1% output coupler, the maximum mode-locked power was 1.2 W with the slope efficiency of 44.7%.

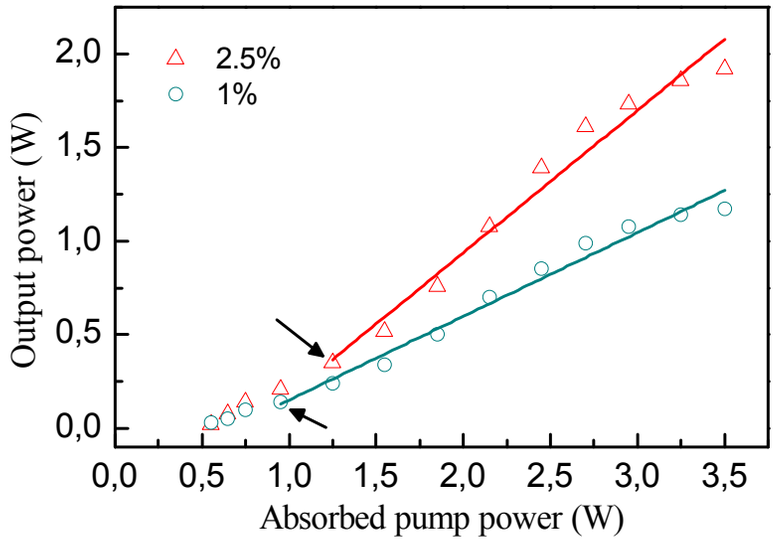


Figure 18. Average output power versus absorbed pump power of the mode-locked Yb:YAG ceramic laser with output couplings of 2.5% (triangles) and 1% (circles). The cw mode-locking thresholds are indicated by arrows.

At the highest output power, the pulse duration was measured to be 418 fs ($sech^2$ assumption). The FWHM width of the spectrum was 3.4 nm at the central wavelength of 1048 nm (Figure 19 left). The radio-frequency spectrum was also measured by an electrical spectrum analyzer to characterize the performance of femtosecond pulse train at the high power operation. As depicted by Figure 19, the spectrum shows a clean peak at a repetition rate of 64.27 MHz without side peaks, implying that the Q-switching instabilities have been fully depressed. A wider acquisition frequency span (from 0 to 300 MHz with 100 kHz resolution bandwidth) was also performed (inset in Figure 19 right), which was a clear indication for the single-pulse operation in high output power level. The results presented above definitely affirmed that the Yb:YAG ceramic is an excellent laser medium for high-power and high-efficiency diode-pumped ultrafast lasers and amplifiers.

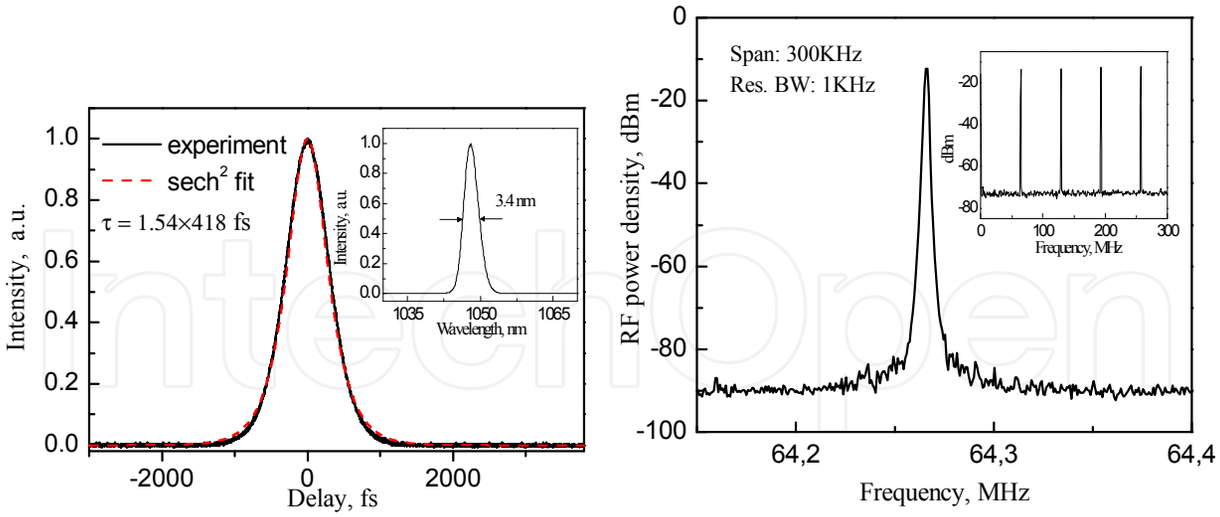


Figure 19. Left, intensity autocorrelation trace of the mode-locking laser pulses with 1.9 W average power; inset, the corresponding spectrum. Right, the rf spectrum at fundamental repetition frequency of the 418 fs pulse train; inset, resolution bandwidth of 100 kHz and span of 300 MHz.

With a similar experimental layout as depicted in Figure 17, a cw mode-locked picosecond Yb:LSO laser was also realized with a 5% doped 3-mm-thick Yb^{3+}:Lu_2SiO_5 crystal as the laser medium [5.22]. At the pump power of 5.4 W from the fiber coupled diode laser, 0.72 W stable mode-locked pulses were obtained with an output coupler of 1% transmittivity. However, the thermal loading prevented higher output power when the pump power increased. The central wavelength of the mode-locked pulses lay on 1058 nm with a FWHM bandwidth of 3.5nm. The pulse duration was 5.1 ps, as shown in Figure 20.

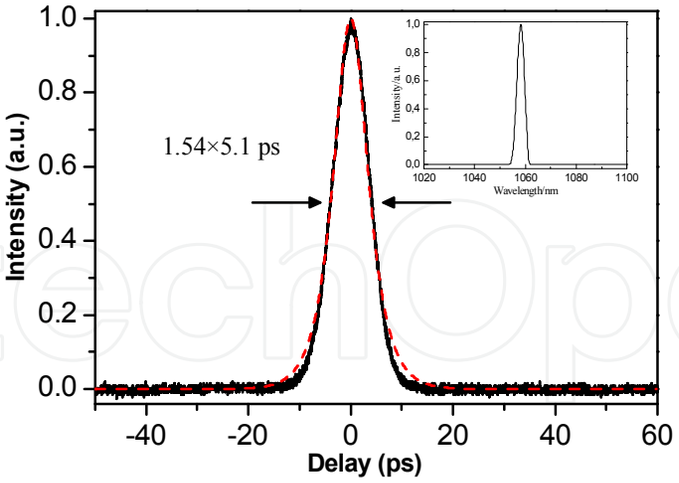


Figure 20. Intensity autocorrelation trace of the mode-locking laser pulses; inset, the corresponding spectrum.

5.3. Femtosecond Yb:GYSO laser

Yb^{3+}-doped $GdYSiO_5$ (Yb:GYSO), a promising ytterbium-doped crystal, has shown several attractive advantages compared to many recent Yb-doped materials. It exhibits $^2F_{7/2}$ ground

state splitting as high as 995 cm^{-1}, which makes the population of the transition lower level much less sensitive to the temperature. Yb:GYSO crystal also possesses a comparatively high fluorescence life time of 1.92 ms and good mechanical properties. Du et al. demonstrated the first efficient tunable CW Yb:GYSO laser operation [5.1], and the picosecond Yb:GYSO laser was reported by another group later [5.2]. We describe here the realization of a femtosecond Yb:GYSO laser [5.3]. The setup for the laser is shown in Fig.21. A 3-mm-long, 5%-doped Yb:GYSO crystal is pumped by a CW Ti:sapphire laser at the wavelength of 976 nm. Three pieces of curved folding mirrors with the radius of curvature (ROC) of 100mm (M1-M3) are used to reduce the beam waist inside the active medium and on the SESAM. The SESAM was designed for 0.4% modulation depth and saturation fluence of 120 $\mu J/cm^2$. Its nonsaturable loss was specified to be 0.3%, and the relaxation time less than 500 fs. A pair of chirped mirrors (CM1, CM2) were used in another arm of the cavity for group velocity dispersion compensation. The chirped mirrors were designed with GDD of -120 fs^2 per bounce within the wavelength range from 1000 nm to 1200 nm. Considering the amount of positive GDD introduced by the 3-mm-long 5%-doped Yb:GYSO crystal [5.4], the net intra-cavity GDD was remained at minus value by introducing two bounces onto the chirped mirrors.

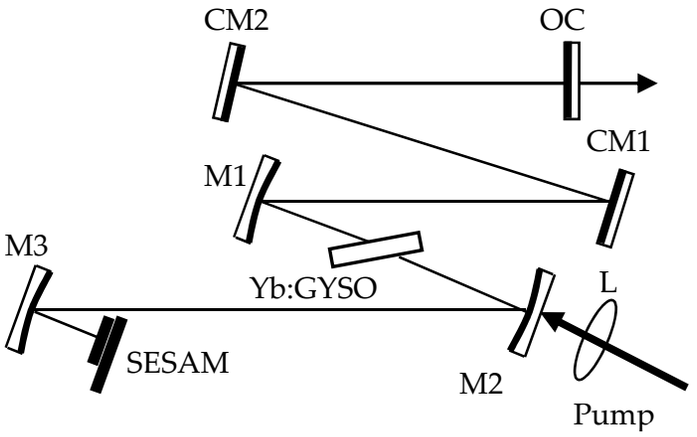


Figure 21. Cavity used to study the femtosecond laser performance of Yb:GYSO. M1, M2, M3, ROC 10 cm; CM1, CM2, flat chirped mirrors; L, lens f=100 mm; OC, 1% output coupler.

With a piece of high reflective mirror in one arm replacing the M3 and SESAM, and removing the chirped mirrors, the CW lasing performance was tested first. At CW lasing, the measured threshold incident pump power was as low as 180 mW, which can be thanks to the large ground state splitting of Yb:GYSO crystal. Output power of 920 mW with diffraction-limited beam pattern was obtained at the wavelength of 1091 nm under 2 W pump power. A tunable range of about 77 nm (from 1033 to 1110nm) was obtained by inserting a Lyot filter in the CW cavity.

After optimization of the cavity alignment shown in Fig. 21, stable and self-starting femtosecond pulses were realized. The autocorrelation trace of the mode-locked pulses is shown in Fig 22(a), the FWHM width of the autocorrelation trace is about 324 fs. If a $sech^2$-pulse shape is assumed, the mode-locked pulse duration is 210 fs.

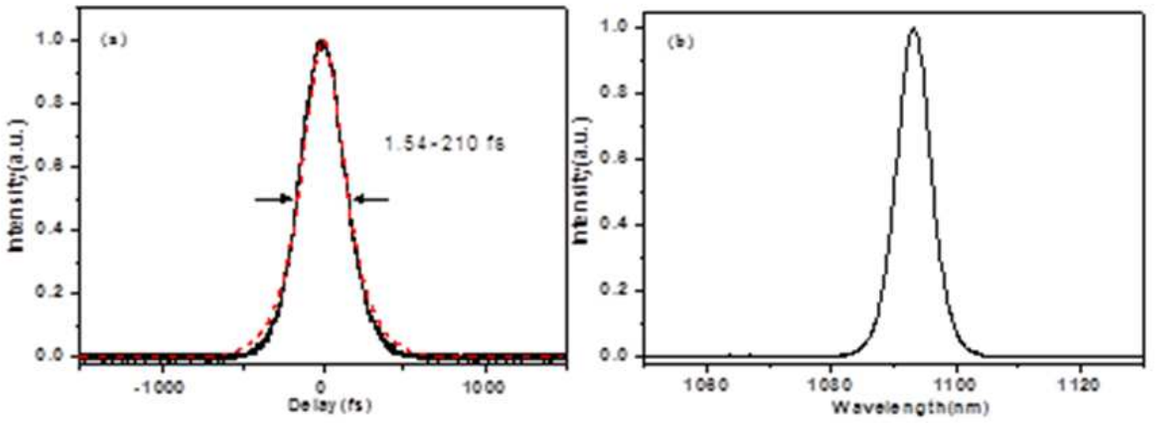


Figure 22. (a) Typical intensity autocorrelation trace of the pulses. The experimental data are shown by the solid curve and the sech2-fitting curve by the dashed curve. (b) The laser spectrum of mode-locking operation.

The spectral width (FWHM) of the pulses was measured as 6.4 nm at the central wavelength of 1093 nm. Fig. 22(b) shows the typical spectrum, compared with the one in CW mode, the central wavelength red shifted slightly from the peak wavelength. The time-bandwidth product is 0.34, which is close to the value of 0.315 for the transform-limited $sech^2$-pulse. This indicates that almost transform-limited pulses were directly obtained from the cavity. However, the gain bandwidth was not fully covered by the obtained spectrum, especially in the shorter wavelength. That means the gain of Yb:GYSO crystal is not fully exploited. Considering the 77 nm tunability achieved in the CW mode, even shorter femtosecond pulses should be possible. Under the full pump power of 2 W from the CW Ti:sapphire laser, the average mode-locking power output from the Yb:GYSO laser was 300 mW at a repetition rate of 80 MHz, corresponding to an energy per pulse of 3.75 nJ and a peak power of 17.9 KW.

A higher mode-locking laser power can be possible by replacing the pump laser by a high power diode laser at 976 nm. In view of the excellent mechanical properties of the Yb:GYSO crystal, a new kind of femtosecond laser with high output power and compactness is very promising.

5.4. Picosecond and femtosecond Yb:YGG laser

Yttrium gallium garnet (YGG) is another garnet crystal. Similar to YAG and GGG, $Y_3Ga_5O_{12}$ (YGG) has many desirable advantages for laser materials—stable, hard, optically isotropic, having good thermal conductivity (9 W/mK), and accepting substitutionally trivalent ions of both rare-earth and iron groups [4.8]. Yb^{3+} doped yttrium gallium garnet (Yb:YGG) was first reported as a scintillator [5.23-24]. The most interesting property is that the bandwidth of its emission spectrum is nearly four times boarder than Yb:YAG 's [5.23]. The high-quality Yb:YGG crystal suitable for laser operation had been grown though optical floating zone method by H. Yu et al for the first time [5.25], and the special thermal properties, including the specific heat, thermal expansion coefficient, thermal diffusion coefficient, and thermal

conductivity had been investigated. Tab.3 shows properties comparisons of Yb:YGG, Yb:YAG and Yb:GGG [5.25]. In this section, we reviewed the diode pumped passively mode-locked Yb:YGG laser [5.26-27].

Crystals	Yb:YGG (10at%)	Yb:YAG	Yb:GGG
Symmetry	Cubic	Cubic	Cubic
Thermal expansion coefficient (10^{-6} K^{-1})	3.8	8.18 (10at%)	~7 (Pure)
Specific Heat (J/gK)	0.43	~0.63 (10at%)	~0.37 (Pure)
Thermal diffusion coefficient (mm^2s^{-1})	1.33	1.62 (10at%)	~3 (Pure)
Thermal Conductivity (W/m·K)	3.47	~4.8 (10at%)	7.5 (Pure)
Absorption Cross-sections ($10^{-20}cm^2$)	2.7 (970 nm)	0.77 (941 nm)	0.6 (945 nm)
Emission Cross-sections ($10^{-20}cm^2$)	2.6 (1025 nm)	2.03 (1031 nm)	1.1 (1031 nm)
FWHM at emission peak	22 nm	10 nm	~10 nm
Positive band at effective gain cross-sections (β=0.5)	120 nm	~100 nm	~80 (nm)

Table 3. Comparisons of Yb:YGG, Yb:YAG and Yb:GGG

The Yb:YGG single crystal employed in the experiment was grown by the optical floating zone method, which was fine polished and antireflection coated at a broad spectrum range around 1 μm with cross section of 3 mm×3 mm and length of 3.2 mm. A high brightness fiber-coupled diode laser emitting at 970 nm (Jenoptik, JOLD-7.5-BAFC-105) was used to end-pump the laser medium. The pump laser output from the fiber (with 50 μm core diameter and 0.22 numerical aperture) was coupled into the laser crystal where the laser spot radius was about 30 μm. Fig. 23 (a) is the schematic of the pumping geometry and laser cavity. A Z-fold cavity was employed for mode-locking experiment. M1 was a plane dichroic mirror with high transmission at 970 nm and high reflection at 1020-1100 nm; M2, M3 and M4 were concave mirrors, with radii of curvature of 300 mm, 200 mm and 200 mm, respectively. Passive mode-locking was realized by using a semiconductor saturable absorber mirror (SESAM) (BATOP), which has a saturable absorption of 0.4 % at 1040 nm, a saturation fluence of 120 μJ/cm^2, relaxation time less than 500 fs, and non-saturable loss of less than 0.3 %. A plane-wedged mirror with transmission rate of 2.5 % was used as the output coupler (OC). According to the ABCD matrix, the cavity was very stable and had large parameter space. After optimization of the cavity alignment, laser pulses as short as 2.1 ps were generated with an average power more than 1 W under incident pumping power of 5.5 W, where multi-pulse will interrupt the stable mode-locking operation when pumping power was higher than 5.5 W.

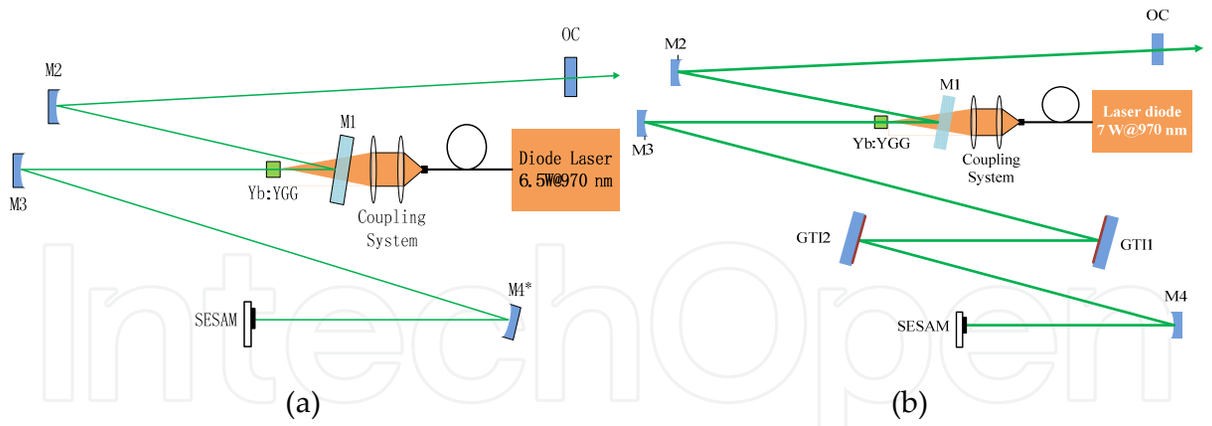


Figure 23. (a) experiment layout of the picoseconds Yb:YGG laser; (b) experiment layout of the femtoseconds Yb:YGG laser

In order to obtain very short pulses, dispersion conversation is an important issue. A pair of Gires–Tournois interferometer (GTI) mirrors, with group-velocity dispersion of -1400 fs^2 per bounce within the wavelength range from 1025 to 1045 nm, was used for dispersion compensation, as shown in Fig. 23 (b). Limited by the available pump power, the maximum output power was 570 mW under 6.9 W of incident pump power. We measured the intensity autocorrelation trace by using the commercial noncollinear autocorrelator (Femtochrome, FR-103MN). As shown in Fig. 24 (a), the FWHM width of the autocorrelation trace was about 360 fs. If a $sech^2$-pulse shape was assumed, the mode-locked pulse duration was 245 fs. The Fig. 24 (b) depicts the corresponding spectrum of the stable mode locking, which had a FWHM bandwidth of 5.8 nm at the central wavelength of 1045 nm. The time-bandwidth product was calculated to be 0.39.

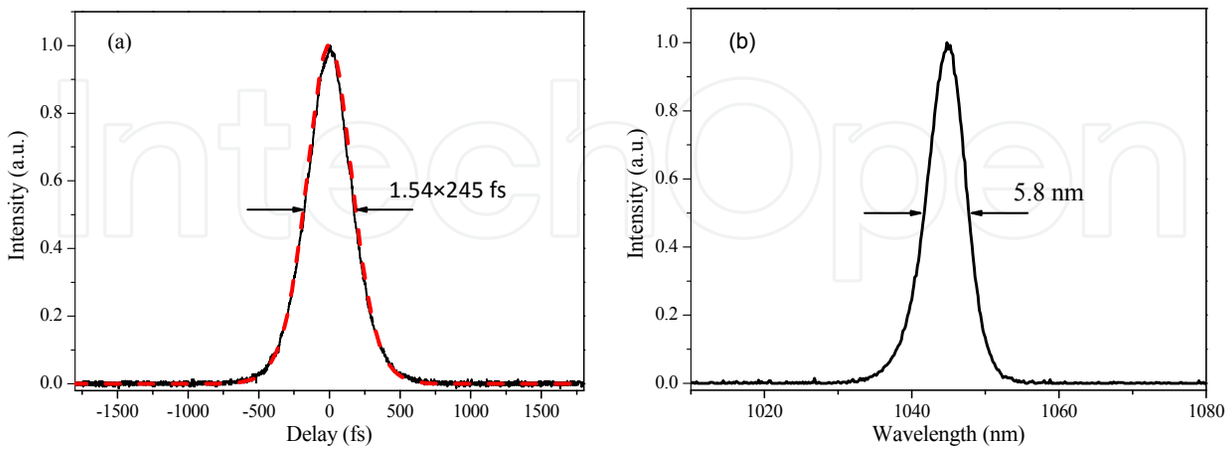


Figure 24. (a) Intensity autocorrelation trace of the pulse. The experimental data are shown by the solid curve and the $sech^2$-fitting curve by the dashed curve. (b) The laser spectrum of mode-locking operation.

6. Mode-locked femtosecond Cr^{4+}-doped laser

After several decades of development, there are many kinds of gain media which can operate in near infrared region, but only a few of them can be used in mode-locked lasers. In chapters 4 and 5, Nd-doped and Yb-doped mode-locked lasers have been described. Most Nd-doped lasers work in picosecond region, so do some Yb-doped lasers. Although some Yb-doped lasers can deliver femtosecond pulses, the generated spectral bandwith is relatively narrow and can't support very short pulses.

There are two chromium doped media, namely chromium doped forsterite (Cr^{4+}:Mg_2SiO_4) and chromium doped yttrium aluminium garnet (Cr^{4+}:YAG), are very attractive for femtoseond laser application. They have very broad emission range which can support few tens of femtoseond pulse generation. Combined with the interesting wavelength ranges they cover (1.3 and 1.5 μm, respectively), these lasers have find wide applications in optical communication [6.1], optical coherence tomography [6.2], biophotonics [6.3] and so on. In this section, we will present our work on the development of these two kind of ultrafast lasers.

6.1. Efficient femtoseond Cr:forsterite laser

Forsterite is an anisotropic crystal belonging to the orthorhombic space group. Cr^{4+}:forsterite crystal shows many excellent characteristics as a laser gain medium. Some important parameters are listed in Table 4 and compared with those of Ti:sapphire crystal. Except for low thermal conductivity and relatively small emission cross section, other physical parameters of Cr^{4+}:forsterite crystal are comparable with those of Ti:sapphire crystals. The Cr^{4+}:forsterite crystal can support the generation of very short femtosecond pulses.

Crystal name	Ti:Sapphire	Cr:Forsterite
Density (g/cm^3)	3.98	3.217
Melt point (℃)	2050	1895
Moh's hardness	9	7
Thermal conductivity (W/(m·k))	33	8
Thermal expansion (K^{-1})	5×10^{-6}	9.5×10^{-6}
Tuning range (nm)	660~1050	1130~1367
Upper level lifetime (us)	3.2	2.7
Emission cross section (cm^2)	4×10^{-19}	1.44×10^{-19}
Center wavelength (nm)	795	1244(cw),1235(pulsed)
Shortest pulse width ever achieved (fs)	<5 fs[6.4]	14 fs[6.5]

Table 4. Parameter comparison of Ti:sapphire and Cr:forsterite

Cr^{4+}:forsterite has very wide absorption and emission spectrum, as shown in Figure 25. The use of absorption peaks at 470 nm and 730 nm are typically excluded due to lack of pump sources. The relatively lower but much wider peak near 1 μm is preferred because of the vast availability of the pump laser. Besides, the quantum defect in the crystal will be much

smaller when pumped at this wavelength. Although the emission spectrum extends from 600 nm to 1400 nm, wavelengths below 1100 nm overlaps with the absorption spectrum and suffers significant reabsorption, which prevents stimulated emission. Only the part above 1100 nm is suitable for laser operation. Up to now, the shortest pulse duration with Cr^{4+}: forsterite laser of 14 fs was achieved with 80 mW output power [3.49]. We'll present our work on the development of highly efficient self-starting femtosecond Cr:forsterite laser here. With a 7.9 W Yb doped fiber laser as the pump, we obtained stable femtosecond laser pulses with an average power of 760 mW, yielding a pump power slope efficiency of 12.3% [6.6].

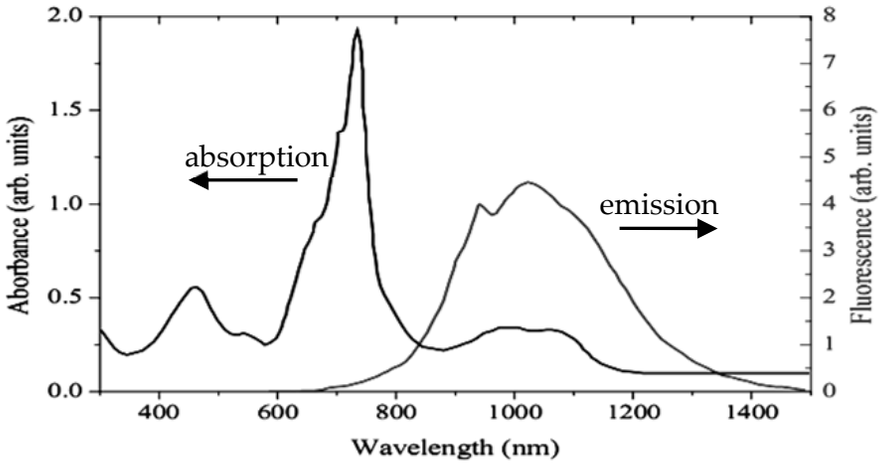


Figure 25. Absorption and emission spectrum of Cr^{4+}:forsterite

The schematic diagram of an efficient Cr^{4+}:forsterite laser is shown in Figure 26 A 1064 nm linearly polarized cw fiber laser is used as the pump (AYDLS-PM-10, Amonics), which deliver 7.9 W average power at maximum. The dimension of Cr^{4+}:forsterite crystal is 4 mm× 2 mm×9 mm and the crystal is cut for propagation of light along the a axis and emitting beam polarization along the c axis (P_{mnb} notation). Both ends are cut at Brewster's angle and polished in order to reduce the reflective loss to the minimum. Due to the low thermal conductivity, the crystal is wrapped in thin indium foil and tightly held in a copper holder. A thermoelectric cooler cools the holder down to 5℃. Although lower temperature can bring higher output power, water condensation on crystal surface will induce unstable operation.

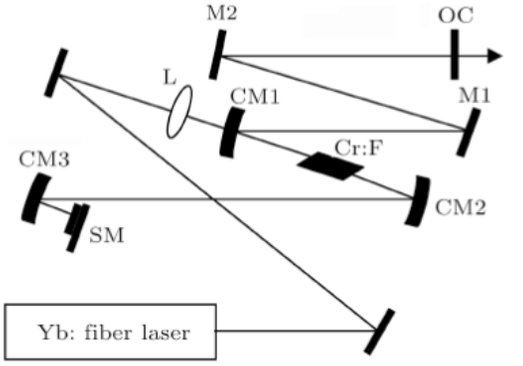


Figure 26. Schematic of the femtosecond Cr:forsterite laser. CM1–CM3: Chirped mirrors, ROC 100 mm; M1 and M2: plane chirped mirrors.

In order to obtain femtosecond pulses, dispersion compensation is important, especially when the used laser crystal is relatively long. By using the formula 13[6.8], the group-delay dispersion of Cr^{4+}:forsterite is calculated and shown in Figure 27.

$$GDD = \frac{1}{2\times 5.17}\left[2\times 84.42 + 6\times 116.70(\omega-\omega_0) + 12\times(-101.21)(\omega-\omega_0)^2 + 20\times 125.08(\omega-\omega_0)^3\right] \quad (13)$$

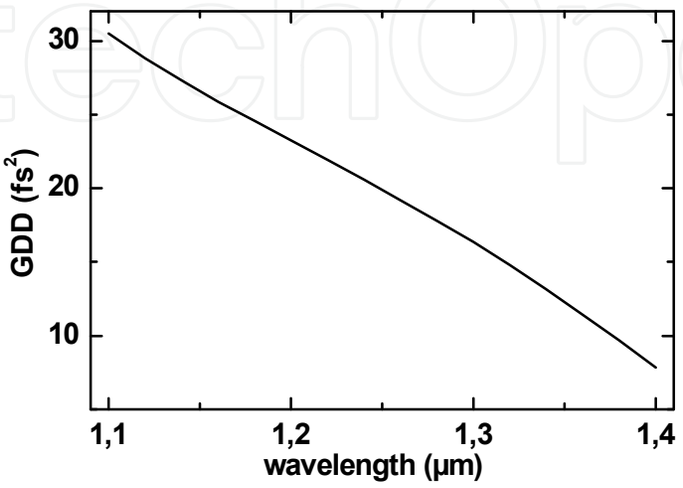


Figure 27. Group-delay dispersion from 1 mm Cr^{4+}:forsterite crystal

The 9 mm long Cr^{4+}:forsterite crystal introduces about 150 fs^2 positive GDD. In order to compensate these dispersion, all the reflective mirrors in cavity are chirped mirrors except the 3% output coupler (OC) and the saturable mirror (SM). Each bounce on CM1, CM2 and CM3 brings in -60±20 fs^2, and -70±20 fs^2 on M1 and M2, respectively. Considering the positive GDD introduced by 1.8-m-long air, the final net intra-cavity GDD after one single trip is about -130 fs^2. Due to the strong oscillations in negative GDD introduced by all the chiped mirrors, a certain amount of negative GDD is necessary to insure the stable mode locking. The semiconductor saturable absorber mirror (SESAM), which is highly reflectively coated from 1240 nm to 1340 nm, has a modulation depth of 2.5% and saturable fluence of 70 $\mu J/cm^2$. In order to reduce the inserting losses, we chose a nonsaturable loss of the SESAM less than 0.5%.

A lens with the focal length of 100 mm is used to focus the pump beam into the crystal. In order to achieve good matching and overlapping between pump and resonant beam, the radius of curvature (ROC) of CM1 and CM2 are 100 mm. Besides, because stable mode locking requires sufficient energy fluence on SESAM, CM3 with ROC of 100 mm is used to focus the resonant beam on it.

The relationship between pump power and output power is shown in Figure 28. The pump power threshold for stable mode locking is 1.8 W, with corresponding output power of 49 mW. The maximum output power of 760 mW is obtained when pump power increases to 7.9 W, which indicates record high slope efficiency as 12.3%. When optimizing the output power of mode-locking operation, we found that a slightly adjustment of the concave mirror

CM2 was necessary when the laser cavity was firstly optimized at other pump powers. We contribute this to the thermal loading effect in the laser crystal. The mode-locking power of the Cr:forsterite laser was almost linear till the pump power up to 7.9 W. Hence we believe that even higher output power can be expected if we use a pump laser with higher power.

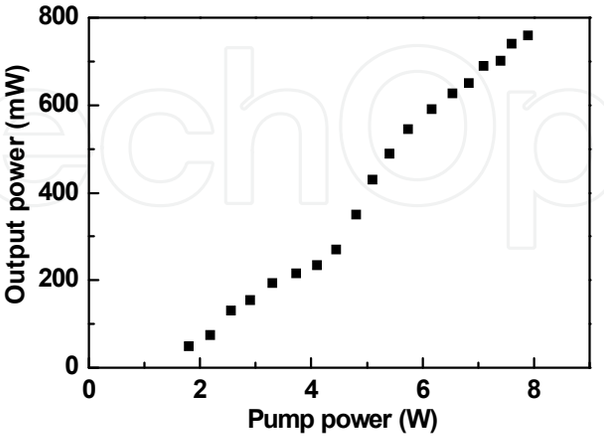


Figure 28. Variation of the mode locking output power as a function of the pump power.

The intensity autocorrelation trace (measured by a FR-103MN autocorrelator, Femtochrome Research, Inc.) and spectrum (measured by AQ-6315A, ANDO) are shown in Figure 29. The autocorrelation trace captured by an oscilloscope shows a FWHM of 71 fs, which indicates the pulse duration of 46 fs by assuming a $sech^2$ pulse shape. The spectrum of mode locking operation is centered at 1277 nm, with a width of 45 nm. A time-bandwidth product of 0.38 is obtained, indicating that the output pulses are nearly transform limited.

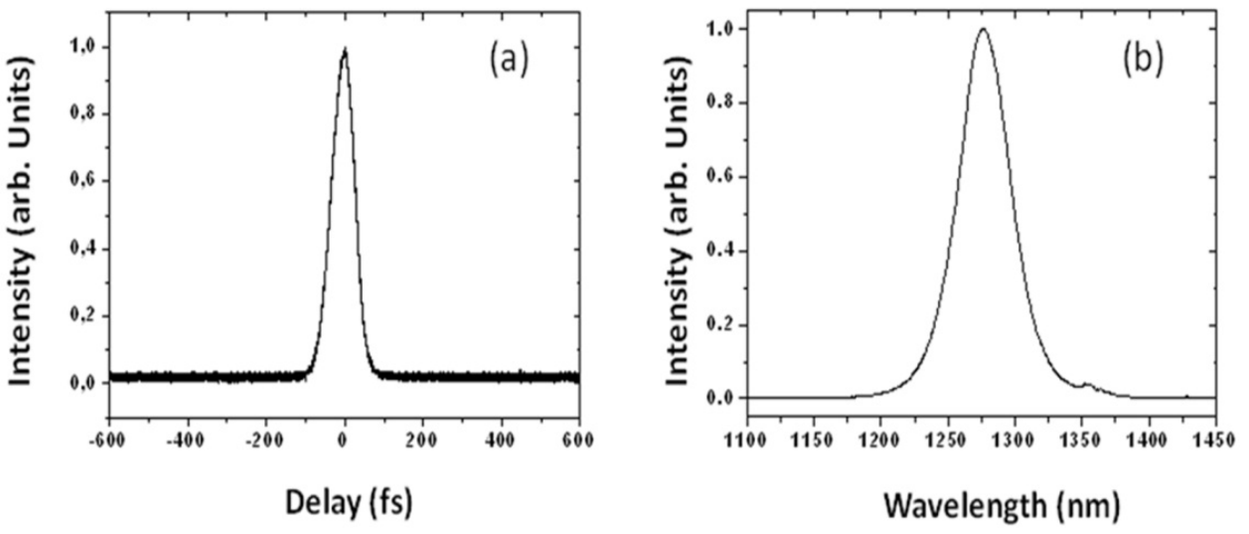


Figure 29. (a) Intensity autocorrelation trace of the output pulses and (b) spectrum of mode locking operation.

The mode-locked Cr^{4+}: forsterite laser can stably work for hours if the environment is dry and stable. The most probable factor which disturbs the mode locking is the water

condensation on crystal surfaces. If the environment is quite humid, nitrogen blowing or dehumidifier is required. Based on this efficient femtosecond Cr:forsterite laser, we also realized red light femtosecond laser output with a intra-cavity frequency-doubled Cr:forsterite laser configuration [6.7].

6.2. Self-starting mode-locked femtosecond Cr^{4+}:YAG laser

Chromium doped yttrium aluminium garnet (Cr^{4+}: YAG) is a remarkable gain medium which generates near infrared laser beam. Moreover, it can support femtosecond laser operation for its wide emission spectrum. The first laser operation in Cr^{4+}: YAG was reported in 1988 [6.9]. In 1993, 26 ps pulses were obtained by using active mode locking [6.10]. So far, femtosecond pulses from Cr^{4+}:YAG can be obtained by active mode locking [6.11], kerr-lens mode locking [6.12-13] and SESAM mode locking [6.14-15]. The record of shortest pulses was reported by Ripin *et al.* in 2002 [6.16].

The absorption spectrum of Cr^{4+}: YAG extends from 950 nm to 1100 nm. It's convenient to use all-solid-state Nd:YAG laser or Yb doped fiber laser as pump source. The emission spectrum extends from 1250 nm to 1650 nm, as shown in Figure 30. Although the peak is at 1.39 μm, the most reported output wavelengths are near 1.5 μm.

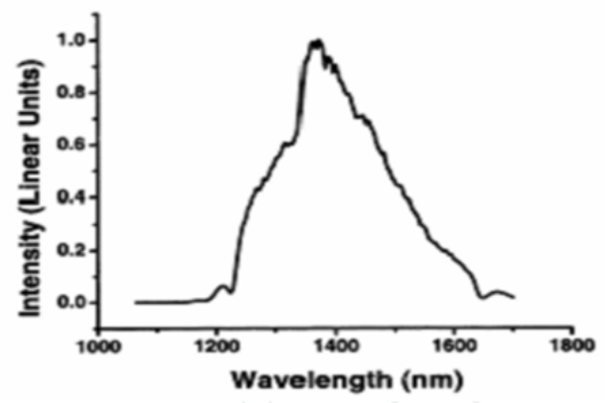


Figure 30. Emission spectrum of Cr^{4+}:YAG

Cr^{4+}:YAG is suitable to generate femtosecond pulses near 1.5 μm for its wide emission spectrum and some other characteristics. There are still some obvious drawbacks though. First, the thermal conductivity is relatively low. The severe thermal lens effect is an annoying problem which causes the unstability of the intra-cavity laser modes. Second, the pump beam and resonant beam both suffer re-absorption effect, which decreases the pump efficiency and increases intra-cavity loss. However, The Cr^{4+}:YAG crystal is still a good gain medium in near infrared range near 1.5 μm. It can support femtosecond pulses generation and has the potential to be used in optical fiber communication, femtobiology, femtochemistry and so on. In this section, a very compact and self-starting femtosecond Cr^{4+}:YAG laser with a pulse width of 65 fs was described [6.17].

The schematic diagram of self-starting mode locking Cr^{4+}:YAG laser is shown in Figure 31.

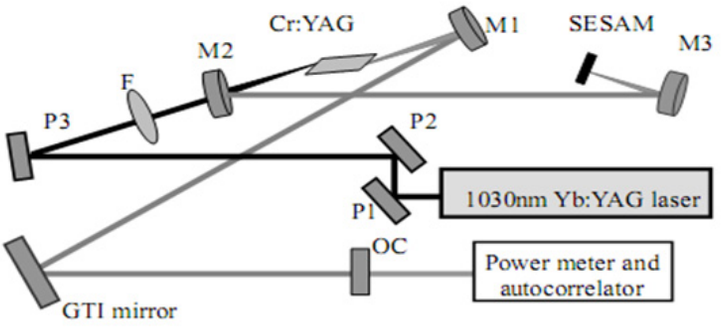


Figure 31. The schematic diagram of the self-starting mode locking Cr^{4+}: YAG laser.

M1, M2 and M3 are concave mirrors with ROC=100 mm, anti-reflective coated (T>98%) at 870~1050 nm and highly-reflective coated (R>99.9%) at 1420~1720 nm. A Gires-Tournois interferometer (GTI) mirror compensates the group-delay dispersion, which can introduce -500±50 fs^2 GDD for each bounce. In order to avoid high intra-cavity loss, an output coupler (OC) with a transmission rate of 1% is used. The pump laser is a commercial Yb:YAG laser which delivers horizontally polarized beam at 1030 nm. The Brewster's angle cut Cr^{4+}:YAG crystal rod is 20 mm long and has a diameter of 5 mm. The laser medium absorbs 90% of the pump energy in this experiment. To reduce the thermal lens effect, the crystal is wrapped in thin indium foil and tightly held in a copper holder. Recirculated cooling water keeps the temperature at 10℃.

For a 20-mm-long Cr^{4+}:YAG, the GDD can be calculated by the following formula [6.12]:

$$GDD = -15296 + 119.83\nu - 0.2054\nu^2 \tag{14}$$

The crystal introduces positive GDD of 226.8 fs^2 at 1500 nm for each single pass. Considering the GDD introduced by air, after compensated by GTI mirror, the net GDD is about -230 fs^2 per single pass in the cavity, as shown in Figure 32. The main drawback by using GTI mirror is that the dispersion compensation isn't precisely adjustable as by using prisms. However, using GTI mirror avoids additional insertion loss and makes the cavity structure more compact and robust.

Under pump power of 9 W, stable mode locked pulses are obtained by fine adjusting the positons of M1, M2, Cr^{4+}:YAG crystal and the SESAM. The highest output power is 95 mW, indicating low slope efficiency. As mentioned before, the re-absorption effect causes large loss for resonant laser. Besides, the OC with low transmission rate also limits the output power. OCs with higher transmission rate are tested, but stable mode locking is unable to achieve.

The mode locking spectra and interferometric autocorrelation trace of output pulses are shown in Figure 33. In Figure a, the solid curve presents the results when the net intra-cavity dispersion is about -230 fs^2. The corresponding spectrum width (FWHM) is 45 nm, centered at 1508 nm. The dashed curve corresponds to the mode-locking results with a net

intra-cavity dispersion of -720 fs² by using another mirror to reflect the beam on GTI mirror once more. The spectrum width (FWHM) is 34.5 nm and a small blue shift can be observed. An interferometric autocorrelation trace corresponding to the solid spectrum curve is shown in Figure b. By assuming a sech² pulse shape, the pulse duration is 65 fs, indicating a time-bandwith product of $\Delta\nu\Delta\tau = 0.372$.

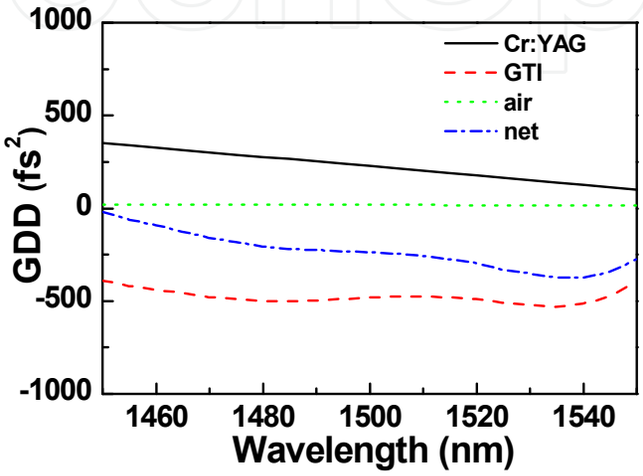


Figure 32. Intra-cavity second-order dispersion contributions.

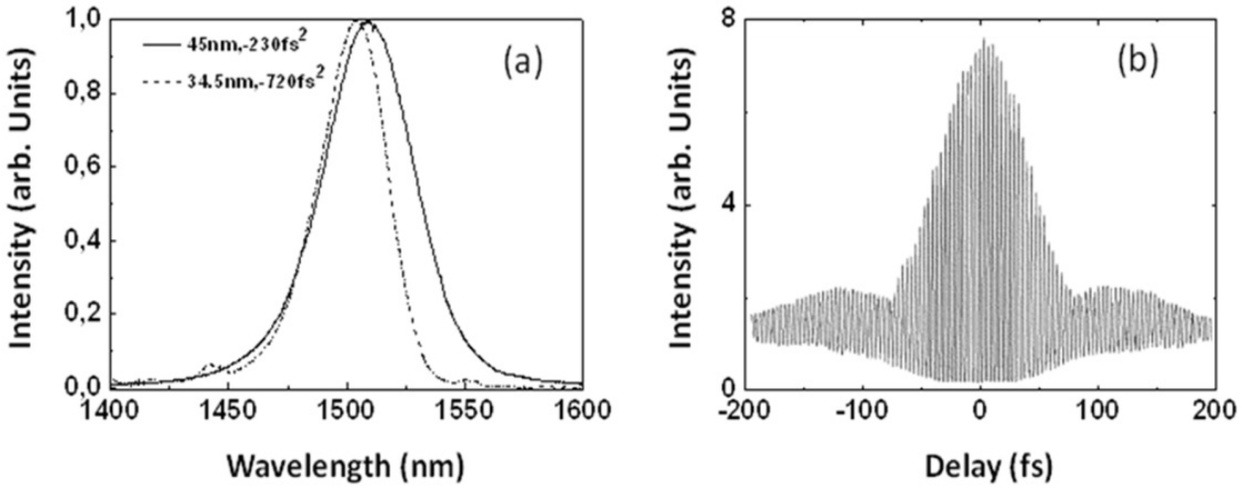


Figure 33. (a) Spectra of mode locking Cr^{4+}:YAG laser, solid curve corresponds to net GDD of -230 fs², dashed curve corresponds to -720 fs²; (b) Interferometric autocorrelation trace of mode locking pulses, the pulse duration is 65 fs.

7. Conclusion

We have described the generation of ultrafast laser pulses with a series of Nd, Yb or Cr-doped gain media. Stable laser pulses were obtained around central wavelengths from 900 nm to 1500 nm and in the picosecond to femtosecond regimes. The pulse duration for Nd-doped mode-locked lasers is in picosecond regime, while for Yb-doped media it can be as short as several tens of femtosecond. The experimental results are summarized in the Table 5. It contains a wide range of very interesting and practically useful all solid-state passively mode-locked ultrafast laser sources in near infrared. Further investigations toward even shorter pulses and higher average power are underway. The direct amplification of all-solid-state ultrafast laser is also in progress toward higher pulse energy.

Gain media	P_{in}(W)/λ_p(nm)	P_{out}(mW)	λ(nm)	Δλ(nm)	Δt
Nd:YVO_4	9W@808	1700	1064		2.3ps
Nd:$GdVO_4$	19.7W@808	128	912		6.5ps
Nd:$LuVO_4$	17W@808	88	916		6.7ps
Nd:GSAG	16.7W@808	510	942.6	0.65	8.7ps
Nd:GGG	24W@808	3200	1062.5	0.25	15ps
	20W@808	320	937.4	0.3	22.7ps
Yb:YAG	2W@940 Ti:S	180	1053	7	170fs
Yb:YAG ceramics	7W@968	1900	1048	3.4	418fs
Yb:GYSO	2W@976 Ti:S	300	1093	6.4	210fs
Yb:LSO	2W@976 Ti:S	70	1047/1066		3.6ps
Yb:YGG	7W@970	570	1045	5.8	245fs
Cr:forsterite	7.9W@1064	760	1277	45	46fs
Cr:YAG	9W@1030	95	1508	45	65fs

Table 5. The experimental results of ultrafast lasers in our lab

Author details

Zhiyi Wei, Binbin Zhou, Yongdong Zhang, Yuwan Zou, Xin Zhong,
Changwen Xu and Zhiguo Zhang
Beijing National Laboratory for Condensed Matter Physics and Institute of Physics, Chinese Academy of Sciences, Beijing, China

Acknowledgments

We thank the helpful technical discussions and support of the laser media by G. L. Bourdet, J.Xu, H.J. Zhang

8. References

[1] U. Keller, K. J. Weingarten, F. X. Kartner, et al, "Semiconductor saturable absorber mirrors (SESAM's) for femtosecond to nanosecond pulse generation in solid-state lasers," IEEE J. Selected Quantum Electron. 2, 435 (1996).

[2] G. J. Spühler, T. Südmeyer, R. Paschotta, M. Moser, K. J. Weingarten and U. Keller, "Passively mode-locked high-power Nd:YAG lasers with multiple laser heads," Appl. Phys. B 71, 19 (2000).

[3] D. Burns, M. Hetterich, A. I. Ferguson, E. Bente, M. D. Dawson, J. I. Davies and S. W. Bland, "High-average-power (>20 W) Nd:YVO_4 lasers mode locked by stain compensated saturable Bragg reflectors," J. Opt. Soc. Am. B 17, 919 (2000).

[4] G. P. A. Malcolm, P. F. Curley and A. I. Ferguson, "Additive pulse modelocking of a diode pumped Nd:YLF laser," Opt. Lett. 15, 1303 (1990).

[5] B. Ileri, C. Czeranowsky, K. Petermann, and G. Huber, "Mixed garnet laser crystals for water vapor detection," in Proceedings of IEEE Conference on Lasers and Electro-Optics Europe, 2005 (IEEE, 2005), p. 10.

[6] T. Kellner, F. Heine, G. Huber, C. Honninger, B. Braun, F. Morier-Genoud, M. Moser, and U. Keller, "Soliton mode-locked Nd:$YAlO_3$ laser at 930 nm," J. Opt. Soc. Am. B 15, 1663 (1998).

[7] A. Schlatter, L. Krainer, M. Golling, and R. Paschotta, D. Ebling, and U. Keller "Passively mode-locked 914-nm Nd:YVO_4 laser," Opt. Lett. 30, 44 (2005).

[8] P. Blandin, F. Druon, F. Balembois, P. Georges, S. Lévêque-Fort and M. P. Fontaine-Aupart, "Diode-pumped passively mode-locked Nd:YVO_4 laser at 914 nm," Opt. Lett. 31, 214 (2006).

[9] J. Aus der Au, D. Kopf, F. Morier-Genoud, M. Moser, and U. Keller, "60-fs pulses from a diode-pumped Nd:glass laser," Opt. Lett. 22, 307 (1997).

[10] C. Hönninger, G. Zhang, U. Keller and A. Giesen, "Femtosecond Yb:YAG laser using semiconductor saturable absorbers," Opt. Lett. 20, 2402 (1995).

[11] M. Weitz, S. Reuter, R. Knappe and R. Wallenstein, "Passive mode-locked 21 W femtosecond Yb:YAG laser with 124 MHz repetition-rate," In Technical Digest of Conference on Lasers and Electro-Optics (optical society of America, Washington, DC, 2004), paper CTucc.

[12] H. Luo, D. Tang, G. Xie, H. Zhang, L. Qin, H. Yu, L. Ng, and L. Qian, "High-power passive mode-locking of a diode pumped Yb:$GdVO_4$ laser," Optics Communications 281, 5382–5384 (2008).

[13] W. Li, Q. Hao, H. Zhai, H. Zeng, W. Lu, G. Zhao, L. Zheng, L. Su, and J. Xu, "Diode-pumped Yb:GSO femtosecond laser," Optics Express 15, 2354–2359 (2007).

[14] F. Thibault, D. Pelenc, F. Druon, Y. Zaouter, M. Jacquemet, and P. Georges, "Efficient diode-pumped Yb^{3+}: Y_2SiO_5 and Yb^{3+}: Lu_2SiO_5 high-power femtosecond laser operation," Opt. Lett. 31, 1555 (2006).

[15] F. Brunner, G. Spühler, J. Au, L. Krainer, F. Morier-Genoud, R. Paschotta, N. Lichtenstein, S. Weiss, C. Harder, A. Lagatsky, and others, "Diode-pumped femtosecond Yb:$KGd(WO_4)_2$ laser with 1.1-W average power," Opt. Lett. 15, 1119–1121 (2000).

[16] F. Brunner, T. Südmeyer, E. Innerhofer, F. Morier-Genoud, R. Paschotta, V. Kisel, V. Shcherbitsky, N. Kuleshov, J. Gao, K. Contag, and others, "240-fs pulses with 22-W average power from a mode-locked thin-disk Yb:KY(WO_4)$_2$ laser," Opt. Lett. 27, 1162–1164 (2002).

[17] U. Griebner, S. Rivier, V. Petrov, M. Zorn, G. Erbert, M. Weyers, X. Mateos, M. Aguiló, J. Massons, and F. Díaz, "Passively mode-locked Yb:KLu(WO_4)$_2$ oscillators," Opt. Express 13, 3465–3470 (2005).

[18] A. Garcia-Cortes, J. M. Cano-Torres, M. Serrano, C. Cascales, C. Zaldo, S. Rivier, X. Mateos, U. Griebner, and V. Petrov, "Spectroscopy and Lasing of Yb-Doped NaY(WO_4)$_2$: Tunable and Femtosecond Mode-Locked Laser Operation," IEEE Journal of Quantum Electronics 43, 758–764 (2007).

[19] F. Druon, S. Chénais, P. Raybaut, F. Balembois, P. Georges, R. Gaum'e, S. Mohr, D. Kopf, and others, "Diode-pumped Yb:$Sr_3Y(BO_3)_3$ femtosecond laser," Opt. Lett. 27, 197–199 (2002).

[20] F. Druon, F. Balembois, P. Georges, A. Brun, A. Courjaud, C. Hönninger, F. Salin, A. Aron, F. Mougel, and others, "Generation of 90-fs pulses from a mode-locked diode-pumped Yb^{3+}:$Ca_4GdO(BO_3)_3$ laser," Opt. Lett. 25, 423–425 (2000).

[21] A. Yoshida, A. Schmidt, V. Petrov, C. Fiebig, G. Erbert, J. Liu, H. Zhang, J. Wang, and U. Griebner, "Diode-pumped mode-locked Yb:YCOB laser generating 35 fs pulses," Opt. Lett. 36, 4425-4427 (2011).

[22] M. Delaigue, V. Jubera, J. Sablayrolles, J. P. Chaminade, A. Garcia, and I. Manek-Hönninger, "Mode-locked and Q-switched laser operation of the Yb-doped $Li_6Y(BO_3)_3$ crystal," Appl. Phys. B 87, 693–696 (2007).

[23] S. Rivier, A. Schmidt, C. Kränkel, R. Peters, K. Petermann, G. Huber, M. Zorn, M. Weyers, A. Klehr, G. Erbert, and others, "Ultrashort pulse Yb:$LaSc_3(BO_3)_4$ mode-locked oscillator," Optics Express 15, 15539–15544 (2007).

[24] M. Lederer, M. Hildebrandt, V. Kolev, B. Luther-Davies, B. Taylor, J. Dawes, P. Dekker, J. Piper, H. Tan, and C. Jagadish, "Passive mode locking of a self-frequency-doubling Yb:$YAl_3(BO_3)_4$ laser," Opt. let. 27, 436–438 (2002).

[25] N. Coluccelli, G. Galzerano, L. Bonelli, A. Di Lieto, M. Tonelli, and P. Laporta, "Diode-pumped passively mode-locked Yb:YLF laser," Optics Express 16, 2922–2927 (2008).

[26] P. Klopp, V. Petrov, U. Griebner, K. Petermann, V. Peters, and G. Erbert, "Highly efficient mode-locked Yb:Sc_2O_3 laser," Opt. let. 29, 391–393 (2004).

[27] U. Griebner, V. Petrov, K. Petermann, and V. Peters, "Passively mode-locked Yb:Lu_2O_3 laser," Opt. Express 12, 3125–3130 (2004).

[28] A. Schmidt, V. Petrov, U. Griebner, R. Peters, K. Petermann, G. Huber, C. Fiebig, K. Paschke, and G. Erbert, "Diode-pumped mode-locked Yb:$LuScO_3$ single crystal laser with 74 fs pulse duration," Opt. let. 35, 511–513 (2010).

[29] F. Druon, F. Balembois, and P. Georges, "Ultra-short-pulsed and highly-efficient diode-pumped Yb:SYS mode-locked oscillators," Opt. Express 12, 5005–5012 (2004).

[30] D. Li, X. Xu, C. Xu, J. Zhang, D. Tang, Y. Cheng, and J. Xu, "Diode-pumped femtosecond Yb: $CaNb_2O_6$ laser," Opt. Lett. 36, 3888–3890 (2011).

[31] Y. Zaouter, J. Didierjean, F. Balembois, G. Lucas Leclin, F. Druon, P. Georges, J. Petit, P. Goldner and B. Viana, "47-fs diode-pumped Yb^{3+}:$CaGdAlO_4$ laser," Opt. Lett. 31,119 (2006).

[32] J. Saikawa, Y. Sato, T. Taira, and A. Ikesue, "Passive mode locking of a mixed garnet Yb: YScAlO ceramic laser," Appl. Phys. Lett. 85, 5845 (2004).
[33] A. Shirakawa, K. Takaichi, H. Yagi, M. Tanisho, J. Bisson, J. Lu, K. Ueda, T. Yanagitani, and A. Kaminskii, "First mode-locked ceramic laser: Femtosecond Yb^{3+}: Y_2O_3 ceramic laser," Laser Phys. 14, 1375–1381 (2004).
[34] M. Tokurakawa, K. Takaichi, A. Shirakawa, K. Ueda, H. Yagi, S. Hosokawa, T. Yanagitani, and A. Kaminskii, "Diode-pumped mode-locked Yb^{3+}:Lu_2O_3 ceramic laser," Opt. Express 14, 12832–12838 (2006).
[35] M. Tokurakawa, K. Takaichi, A. Shirakawa, K. Ueda, H. Yagi, T. Yanagitani, and A. A. Kaminskii, "Diode-pumped 188 fs mode-locked Yb:YO ceramic laser," Appl. Phys. Let. 90, 071101 (2007).
[36] H. Yoshioka, S. Nakamura, T. Ogawa, and S. Wada, "Diode-pumped mode-locked Yb:YAG ceramic laser," Opt. Express 17, 8919–8925 (2009).
[37] H. Yoshioka, S. Nakamura, T. Ogawa, and S. Wada, "Dual-wavelength mode-locked Yb:YAG ceramic laser in single cavity," Opt. Express 18, 1479–1486 (2010).
[38] A. Giesen, H. Hügel, A. Voss, K. Wittig, U. Brauch, and H. Opower, "Scalable concept for diode-pumped high-power solid-state lasers," Appl. Phys. B 58, 365–372 (1994).
[39] A. Giesen and J. Speiser, "Fifteen Years of Work on Thin-Disk Lasers: Results and Scaling Laws," IEEE Journal of Selected Topics in Quantum Electronics 13, 598–609 (2007).
[40] T. Südmeyer, C. Kränkel, C. R. E. Baer, O. H. Heckl, C. J. Saraceno, M. Golling, R. Peters, K. Petermann, G. Huber, and U. Keller, "High-power ultrafast thin disk laser oscillators and their potential for sub-100-femtosecond pulse generation," Appl. Phys. B 97, 281–295 (2009).
[41] C. Kränkel, D. J. H. C. Maas, T. Südmeyer, and U. Keller, "Ultrafast Lasers in Thin-Disk Geometry," High Power Laser Handbook, p. 327, 2011.
[42] R. Peters, C. Kränkel, K. Petermann, and G. Huber, "Power scaling potential of Yb: NGW in thin disk laser configuration," Appl. Phys. B 91, 25–28 (2008).
[43] K. Petermann, D. Fagundes-Peters, J. Johannsen, M. Mond, V. Peters, J. Romero, S. Kutovoi, J. Speiser, and A. Giesen, "Highly Yb-doped oxides for thin-disc lasers," Journal of crystal growth 275, 135–140 (2005).
[44] C. Baer, C. Kränkel, C. Saraceno, O. Heckl, M. Golling, T. Südmeyer, R. Peters, K. Petermann, G. Huber, and U. Keller, "Femtosecond Yb:Lu_2O_3 thin disk laser with 63 W of average power," Opt. lett. 34, 2823–2825 (2009).
[45] C. R. E. Baer, C. Kränkel, C. J. Saraceno, O. H. Heckl, M. Golling, R. Peters, K. Petermann, T. Südmeyer, G. Huber, and U. Keller, "Femtosecond thin-disk laser with 141 W of average power," Opt. Lett. 35, 2302–2304 (2010).
[46] C. Kränkel, J. Johannsen, R. Peters, K. Petermann, and G. Huber, "Continuous-wave high power laser operation and tunability of Yb:$LaSc_3(BO_3)_4$ in thin disk configuration," Appl. Phys. B 87, 217–220 (2007).
[47] O. Heckl, C. Kränkel, C. Baer, C. Saraceno, T. Südmeyer, K. Petermann, G. Huber, and U. Keller, "Continuous-wave and modelocked Yb: YCOB thin disk laser: first demonstration and future prospects," Opt. Express 18, 19201–19208 (2010).

[48] S. Ricaud, A. Jaffres, P. Loiseau, B. Viana, B. Weichelt, M. Abdou-Ahmed, A. Voss, T. Graf, D. Rytz, M. Delaigue, E. Mottay, P. Georges, and F. Druon, "Yb:$CaGdAlO_4$ thin-disk laser," Opt. Lett. 36, 4134–4136 (2011).
[49] N.V. Kuleshov, V.G. Shcherbitsky, V.P. Mikhailov, S. Hartung, T. Danger, S. Kück, K. Petermann, G. Huber, "Excited-state absorption and stimulated emission measurements in Cr^{4+}:forsterite, " J. Lumin. 75, 319 (1997).
[50] C. Chudoba, J. G. Fujimoto, E. P. Ippen, H. A. Haus, U. Morgner, F. X. Kärtner, V. Scheuer, G. Angelow and T. Tschudi, "All-solid-state Cr:forsterite laser generating 14-fs pulses at 1.3 μm," Opt. Lett. 26, 292 (2001).
[51] D. J. Ripin, C. Chudoba, J. T. Gopinath, J. G. Fujimoto, E. P. Ippen, U. Morgner, F. X. Kärtner, V. Scheuer, G. Angelow and T. Tschudi, "Generation of 20-fs pulses by a prismless Cr^{4+}:YAG laser," Opt. Lett. 27, 61 (2002).
[52] http://www.coherent.com.
[53] F. Kallmeyer, M. Dziedzina, X. Wang, H. J. Eichler, C. Czeranowsky, B. Ileri, K. Petermann, and G. Huber, "Nd:GSAG-pulsed laser operation at 943 nm and crystal growth," Appl. Phys. B 89, 305-310 (2007).
[54] C. D. Brandle, Jr. and C. Vanderleeden, "Growth, Optical Properties, and CW Laser Action of Neodymium-Doped Gadolinium Scandium Aluminum Garnet," IEEE J. Quantum Electron. 10, 67 (1974).
[55] S. Wang, X. Wang, F. Kallmeyer, J. Chen, and H. J. Eichler, "Model of pulsed Nd:GSAG laser at 942 nm considering rate equations with cavity structure," Appl. Phys. B 92, 43-48 (2008).
[56] F. Kallmeyer, M. Dziedzina, D. Schmidt, H.-J. Eichler, R. Treichel, and S. Nikolov, "Nd:GSAG laser for water vapor detection by lidar near 942 nm," Proc. SPIE 6451, 64510J (2007).
[57] Changwen Xu, Zhiyi Wei, Yongdong Zhang, Dehua Li, Zhiguo Zhang, X. Wang, S. Wang, H.J.Eichler, Chunyu Zhang and Chunqing Gao, "Diode-pumped passively mode-locked Nd: GSAG laser at 942 nm," Opt. Lett. 34, 2324(2009).
[58] J. E. Geusic, H. M. Marcos, and L. G. Van Uitert, "Laser oscillation in Nd-doped yttrium aluminum, yttrium gallium and gadolinium garnet," Appl. Phys. Lett. 4, 182-184 (1964).
[59] G. F. Albrecht, S. B. Sutton, E. V. George et al, "Solid state heat capacity disk laser ," Laser and Particle Beams 16, 605-625 (1998).
[60] http://www.zlxtech.com.cn/home.asp
[61] M.D. Rotter, C.B. Dane, S. Fochs, K.L. Fortune, R. Merrill, B. Yamamoto, "Solid-state heat-capacity lasers: Good candidates for the marketplace," Photon. Spectra 38, 44-56 (2004).
[62] L. Qin, D. Tang, G. Xie, H. Luo, C. Dong, Z. Jia, H. Yu, and X. Tao, "Diode-end-pumped passively mode-locked Nd:GGG laser with a semiconductor saturable mirror," Opt. Commun. 281, 4762-4764 (2008).
[63] Y. D. Zhang, Z. Y. Wei, C. W. Xu, B. B. Zhou, D. H. Li, Z. G. Zhang, H. H. Jiang, S. T. Yin, Q. L. Zhang, D. L. Sun, "Diode-pumped watt-level mode-locked Nd:GGG laser at 1062 nm," The 7th Asia-Pacitific Laser Symposium, Th-P-78 (2010).
[64] Y. D. Zhang, Z. Y. Wei, C. W. Xu, B. B. Zhou, D. H. Li, Z. G. Zhang, H. H. Jiang, S. T. Yin, Q. L. Zhang, D. L. Sun, "Picoseconds pulse generation with a Nd:GGG laser

operating on quasi-three-level transition," 2009 Lasers & Electro-Optics & the Pacific Rim Conference on Lasers and Electro-Optics, 1-2, 670-671 (2009).

[65] A. Schlatter, L. Krainer, M. Golling, R. Paschotta, D. Ebling and U. Keller, "Passively mode-locked 914-nm Nd:YVO_4 laser," Opt. Lett. 30, 44-46 (2005).

[66] G. J. Spu¨hler, S. Reffert, M. Haiml, M. Moser and U. Keller, "Output-coupling semiconductor saturable absorber mirror," Appl. Phys. Lett. 78, 2733 (2001).

[67] Y. F. Chen, S. W. Tsai, Y. P. Lan, S. C. Wang and K. F. Huang, "Diode-end-pumped passively mode-locked high-power Nd:YVO4 laser with a relaxed saturable Bragg reflector," Opt. Lett. 26, 199-201 (2001)

[68] Ya-Xian Fan, Jing-Liang He, Yong-Gang Wang, Sheng Liu, Hui-Tian Wang and Xiao-Yu Ma, "2-ps passively mode-locked Nd:YVO4 laser using an output-coupling-type semiconductor saturable absorber mirror," Appl. Phys. Lett. 86, 101103 (2005).

[69] Marie-Christine Nadeau, Stéphane Petit, Philippe Balcou, Romain Czarny, Sébastien Montant, and Christophe Simon-Boisson, "Picosecond pulses of variable duration from a high-power passively mode-locked Nd:YVO4 laser free of spatial hole burning," Opt. Lett.35, 1644-1646 (2010).

[70] Y. L. Jia, Z. Y. Wei, J. A. Zheng, W. J. Ling, Y. G. Wang, X. Y. Ma, Z. G. Zhang, "Diode-pumped self-starting mode-locked Nd:YVO4 laser with semiconductor saturable absorber output coupler," Chin. Phys. Lett. 21, 2209 (2004).

[71] Y. L. Jia, W. J. Ling, Z. Y. Wei, Y. G. Wang, X. Y. Ma, "Self-starting passively mode-locking all-solid-state laser with GaAs absorber grown at low temperature," Chin. Phys. Lett. 22, 2575(2005).

[72] A. I. Zagumennyi, V. A. Mikhailov, V. I. Vlasov, A. A. Sirotkin, V. I. Podreshetnikov, Yu. L. Kalachev, Yu. D. Zavartsev, S. A. Kutovoi and I. A. Shcherbakov, "Diode-Pumped Lasers Based on $GdVO_4$ Crystal," Laser Phys. 13, 311-318 (2003).

[73] Jin-Long Xu, Hai-Tao Huang, Jing-Liang He, Jian-Fei Yang, Bai-Tao Zhang, Chun-Hua Zuo, Xiu-Qin Yang and Shuang Zhao, "The characteristics of passively Q-switched and mode-locked 1.06 um Nd:$GdVO_4$ laser with V:YAG saturable absorber," Optical Materials 32, 522 – 525 (2010).

[74] Hou-Ren Chen, Yong-Gang Wang, Chih-Ya Tsai, Kuei-Huei Lin, Teng-Yao Chang, Jau Tang, and Wen-Feng Hsieh, "High-power, passively mode-locked Nd:$GdVO_4$ laser using single-walled carbon nanotubes as saturable absorber," Opt. Lett. 36, 1284-1286 (2011).

[75] Gang Zhang, Shengzhi Zhao, Yufei Li, Guiqiu Li, Dechun Li, Kejian Yang and Kang Cheng, "A dual-loss-modulated Q-switched and mode-locked Nd:$GdVO_4$ laser with AOM and V^{3+}:YAG saturable absorber at 1.34 μm," J. Opt. 13, 035202 (2011).

[76] Kejian Yang, Shengzhi Zhao, Jingliang He, Baitao Zhang, Chunhua Zuo, Guiqiu Li, Dechun Li and Ming Li, "Diode-pumped passively Q-switched and modelocked Nd:$GdVO_4$ laser at 1.34 μm with V:YAG saturable absorber," Optics Express 16, 20176-20185 (2008).

[77] A. K. Zaytseva, C. L. Wangb, C. H. Linc, and C. L. Pana, "Robust Diode-End-Pumped Nd:$GdVO_4$ Laser Passively Mode-Locked with Saturable Output Coupler," Laser Physics 21, 2029 – 2035 (2011).

[78] H. W. Yang, H. T. Huang, J. L. He, S. D. Liu, F. Q. Liu, X. Q. Yang, J. L. Xu, J. F. Yang and B. T. Zhang, "High Repetition Rate Passive Q-Switching of Diode-Pumped

Nd:$GdVO_4$ Laser at 912 nm with V^{3+}:YAG as the Saturable Absorber," Laser Physics 21, 66 – 69 (2011).

[79] Fei Chen, Xin Yu, Xudong Li, Renpeng Yan, Cheng Wang, Deying Chen, Zhonghua Zhang and Junhua Yu, "High power diode-pumped passively Q-switched and mode-locking Nd:GdVO4 laser at 912 nm," Optics Communications 284, 635-639 (2011).

[80] C. Zhang, Z. Y. Wei, L. Zhang, C. Y. Zhang, and Z. G. Zhang, "Passively mode-locked Nd:GdVO4 laser at 912nm," Chinese Physics 15, 2606 (2006).

[81] C.W. Xu, Z.Y. Wei, K.N. He, D.H. Li, Y.D. Zhang, Zhiguo Zhang, "Diode-pumped passively mode-locked Nd:GdVO4 laser at 912 nm," Opt. Commun. 281, 4398 (2008).

[82] He Kun-Na, Wei Zhi-Yi, Xu Chang-Wen, Li De-Hua, Zhang Zhi-Guo, Zhang Huai-Jin, Wang Ji-Yang, Gao Chun-Qing, "Passively Mode-Locked Quasi-Three-Level Nd:LuVO4 Laser with Semiconductor Saturable Absorber Mirror," Chin. Phys. Lett. 25, 4286 (2008).

[83] [5.1] J. Du, X. Liang, Y. Xu, R. Li, Z. Xu, C. Yan, G. Zhao, L. Su, and J. Xu, "Tunable and efficient diode-pumped Yb^{3+}:GYSO laser," Opt. Express 14, 3333 (2006).

[84] W. Li, Q. Hao, L. Ding, G. Zhao, L. Zheng, J. Xu, and H. Zeng, "Continuous-wave and passively mode-locked Yb:GYSO lasers pumped by diode lasers," IEEE J. Quantum Electron. 44, 567 (2008).

[85] B. Zhou, Z. Wei, Y. Zhang, X. Zhong, H. Teng, L. Zheng, L. Su, and J. Xu, "Generation of 210 fs laser pulses at 1093 nm by a self-starting mode-locked Yb:GYSO laser," Opt. Lett. 34, 31 (2009).

[86] W. Yang, J. Li, F. Zhang, Y. Zhang, Z. Zhang, G. Zhao, L. Zheng, J. Xu, and L. Su, "Group delay dispersion measurement of Yb:Gd_2SiO_5, Yb:$GdYSiO_5$ and Yb:$LuYSiO_5$ crystal with white-light interferometry," Opt. Express 15, 8486 (2007).

[87] E. Innerhofer, T. Südmeyer, F. Brunner, R. Paschotta, and U. Keller, "Mode-locked high-power lasers and nonlinear optics-a powerful combination," Laser Phys. Lett. 1, 82 (2004).

[88] S. V. Marchese, C. R. E. Baer, A. G. Engqvist, S. Hashimoto, D. J. H. C. Maas, M. Golling, T. Südmeyer, and U. Keller, "Femtosecond thin disk laser oscillator with pulse energy beyond the 10-microjoule level," Opt. Express 16, 6397 (2008).

[89] C. Hönninger, R. Paschotta, M. Graf, F. Morier-Genoud, G. Zhang, M. Moser, S. Biswal, J. Nees, A. Braun, G. A. Mourou, I. Johannsen, A. Giesen, W. Seeber, and U. Keller, "Ultrafast ytterbium-doped bulk lasers and laser amplifiers," Appl. Phys. B 69, 3 (1999).

[90] S. Uemura, and K. Torizuka, "Center-wavelength-shifted passively mode-locked diode-pumped ytterbium(Yb):yttrium aluminum garnet(YAG) laser," Jpn. J. Appl. Phys. 44, L361 (2005).

[91] B. Zhou, Z. Wei, D. Li, H. Teng, and G. Bourdet, "Numerical and experimental investigation of a continuous-wave and passively mode-locked Yb:YAG laser at a wavelength of 1.05 μm," Appl. Opt. 48, 5978 (2009).

[92] Zhou Bin-Bin, Wei Zhi-Yi, LI De-Hua, Teng Hao, Bourdet G. L, "Generation of 170-fs Laser Pulses at 1053nm by a Passively Mode-Locked Yb:YAG Laser," Chin. Phys. Lett. 26, 054208 (2009).

[93] G. L. Bourdet, "Theoretical investigation of quasi-three-level longitudinally pumped continuous wave lasers," Appl. Opt. 39, 966 (2000).

[94] G. L. Bourdet, and E. Bartnicki, "Generalized formula for continuous-wave end-pumped Yb-doped material amplifier gain and laser output power in various pumping configurations," Appl. Opt. 45, 9203 (2006).
[95] R. J. Beach, "CW theory of quasi-three level end-pumped laser oscillators," Opt. Communications 123, 385 (1995).
[96] K. Takaichi, H. Yagi, J. Lu, A. Shirakawa, K. Ueda, T. Yanagitani, and A. A. Kaminskii, "Yb^{3+}-doped $Y_3Al_5O_{12}$ ceramics – a new solid-state laser material," Phys. Status Solidi A 200, R5 (2003).
[97] A. A. Kaminskii, M. Sh. Akchurin, V. I. Alshits, K. Ueda, K. Takaichi, J. Lu, T. Uematsu, M. Musha, A. Shirakawa, V. Gabler, H. J. Eichler, H. Yagi, T. Yanagitani, S. N. Bagayev, J. Fernandez, and R. Balda, "New results in studying physical properties of nanocrystalline laser ceramics," Kristallografiya 48, 562 (2003).
[98] J. Dong, A. Shirakawa, K. Ueda, H. Yagi, T. Yanagitani, and A. A. Kaminskii, "Efficient Yb^{3+}:$Y_3Al_5O_{12}$ ceramic microchip lasers," Appl. Phys. Lett. 89, 091114 (2006).
[99] S. Nakamura, H. Yoshioka, Y. Matsubara, T. Ogawa, and S. Wada, "Efficient tunable Yb:YAG ceramic laser," Opt. Communications 281, 4411 (2008).
[100] H. Yoshioka, S. Nakamura, T. Ogawa, and S. Wada, "Diode-pumped mode-locked Yb:YAG ceramic laser," Opt. Express 17, 8919 (2009).
[101] B. Zhou, Z. Wei, Y. Zou, Y. Zhang, X. Zhong, G. L. Bourdet, and J. Wang, "High-efficiency diode-pumped femtosecond Yb:YAG ceramic laser," Opt. Lett. 35, 288 (2010).
[102] A. Lucca, G. Debourg, M. Jacquemet, F. Druon, F. Balembois, P. Georges, P. Camy, J. L. Doualan, and R. Moncorgé, "High-power diode-pumped Yb^{3+}:CaF_2 femtosecond laser," Opt. Lett. 29, 2767 (2004).
[103] F. Thibault, D. Pelenc, F. Druon, Y. Zaouter, M. Jacquemet, and P. Georges, "Efficient diode-pumped Yb^{3+}:Y_2SiO_5 and Yb^{3+}:Lu_2SiO_5 high-power femtosecond laser operation," Opt. Lett. 31, 1555 (2006).
[104] Zhou Bin-bin, Zou Yu-wan, Li De-hua, Wei Zhi-yi, Zheng Li-he, Su Liang-bi, Xu Jun, "The experimental study of the continuous-wave mode-locked picosecond Yb:LSO laser," Chinese J. Lasers (in Chinese) 36, 1806 (2009).
[105] I. A. Kamenskikh, N. Guerassimova, C. Dujardin, N. Garnier, G. Ledoux, C. Pedrini, M. Kirm, A. Petrosyan, D. Spassky, "Charge transfer fluorescence and f–f luminescence in ytterbium compounds," Opt. Mater. 24, 267–274 (2003).
[106] S. Heer, M. Wermuth, K. Krämer, and H. U. Güdel, "Sharp ^2E upconversion luminescence of Cr^{3+} in $Y_3Ga_5O_{12}$ codoped with Cr^{3+} and Yb^{3+}," Phys. Rev. B 65, 125112 (2002).
[107] H. Yu, K. Wu, B. Yao, H. Zhang, Z. Wang, J. Wang, Y. Zhang, Z. Wei, Z. Zhang, X. Zhang, and M. Jiang, "Growth and characteristics of Yb doped $Y_3Ga_5O_{12}$ laser crystal," IEEE J. Quantum Electron. 46, 1689-1695 (2010).
[108] Y. Zhang, Z. Wei, B. Zhou, C. Xu, Y. Zou, D. Li, Z. Zhang, H. Zhang, J. Wang, H, Yu, K. Wu, B. Yao and J. Wang, "Diode-pumped passively mode-locked Yb:$Y_3Ga_5O_{12}$ laser," Opt. Lett. 34, 3316-3318 (2009).
[109] Y. D. Zhang, Z. Y. Wei, Z. G. Zhang, D. N. Qian, L. Lv, X. D. Zeng, H. J. Zhang, H. H. Yu, J. Y. Wang, "Diode Pumped Efficient Continuous Wave and Picoseconds Yb:YGG Laser," (In Chinese) Chinese Journal of Lases 38, 0202005 (2011).

[110] S. L. Gilbert, W. C. Swann and T. Dennis, "Wavelength standards for optical communications," Proc. SPIE 4269, 184 (2001).
[111] P. R. Herz, Y. Chen, A. D. Aguirre and et al. "Ultrahigh resolution optical biopsy with endoscopic optical coherence tomography," Opt. Express 12, 3532 (2004).
[112] B. E. Bouma, G. J. Tearney, I. P. Bilinsky and et al. "Self-phase-modulated Kerr-lens mode-locked Cr: forsterite laser source for optical coherence tomography," Opt. Lett. 21, 1839 (1996).
[113] H. M. Crespo, J. R. Birge, E. L. Falcão-Filho and et al. "Nonintrusive phase stablization of sub-two-cycle pulses from a prismless octave-spanning Ti:sapphire laser," Opt. Lett. 33, 833 (2008).
[114] C. Chudoba, J. G. Fujimoto, E. P. Ippen and et al. "All-solid-state Cr:forsterite laser generating 14-fs pulses at 1.3 um," Opt. Lett. 26, 292 (2001).
[115] Zhou Bin-Bin, Zhang Yong-Dong, Zhong Xin, Wei Zhi-Yi, "Highly Efficient Self-Starting Femtosecond Cr:Forsterite Laser," Chin. Phys. Lett. 25, 3679 (2008).
[116] Zhong Xin, Zhou Bin-Bin, Zhan Min-Jie, Wei Zhi-Yi, "Generation of Red Light Femtosecond Pulses from an Intra-Cavity Frequency-Doubled Cr^{4+}:Forsterite Laser," Chin. Phys. Lett. 27, 044204 (2010).
[117] I. Thomann, L. Hollberg, S. A. Diddams and R. Equall, "Chromium-doped forsterite: dispersion measurement with white-light interferometry," Appl. Phys. 42, 1661 (2003).
[118] N. B. Angert, N. I. Borodin, V. M. Garmash and et al. "Lasing due to impurity color centers in yttrium aluminum garnet crystals at wavelength in the range 1.35-1.45 um," Sov. J. Quantum Electronics 18, 73 (1988).
[119] P. M. W. French, N. H. Rizvi, J. R. Taylor and A. V. Shestakov, "Continuous-wave mode-locked Cr^{4+}:YAG laser," Opt. Lett. 18, 39 (1993).
[120] A. Sennaroglu, C. R. Pollock and H. Nathel, "Continuous-wave self-mode-locked operation of femtoseond Cr^{4+}:YAG laser," Opt. Lett. 19, 390 (1994).
[121] Y. Ishida and K. Naganuma, "Characteristics of femtosecond pulses near 1.5 um in a self-mode-locked Cr^{4+}:YAG laser," Opt. Lett. 19, 2003 (1994).
[122] Y. P. Tong, J. M. Sutherland, P. M. W. French and et al. "Self-starting Kerr-lens mode-locked femtosecond Cr^{4+}:YAG and picosecond Pr^{3+}:YLF solid-state lasers," Opt. Lett. 21, 644 (1996).
[123] Z. Zhang, T. Nakagawa, K. Torizuka and et al. "Self-starting mode-locked Cr^{4+}:YAG laser with a low loss broadband semiconductor saturable-absorber mirror," Opt. Lett. 24, 1768 (1999).
[124] S. Naumov, E. Sorokin, V. L. Kalashnikov and et al. "Self-staring five optical cycle pulses generation in Cr^{4+}:YAG laser," Appl. Phys. B 76, 1 (2003).
[125] D. J. Ripin, C. Chudoba, J. T. Gopinath and et al. "Generation of 20-fs pulses by a prismless Cr^{4+}:YAG laser," Opt. Lett. 27, 61 (2002).
[126] Zhou Bin-Bin, Zhang Wei, Zhan Min-Jie, Wei Zhi-Yi, "Self-starting mode-locked Cr^{4+}:YAG laser by Gires-Tournois interferometer mirror for dispersion compensation," Acta Physica Sinica (in Chinese), 57, 1742 (2008).